THE PENNSYLVANIA STATE UNIVERSITY
SCHREYER HONORS COLLEGE

DEPARTMENT OF BIOMEDICAL ENGINEERING

THE EFFECTS OF BIOCONJUGATION OF CALCIUM PHOSPHOSILICATE NANOPARTICLES ON THE DELIVERY TO BREAST CANCER CELLS

VIRGINIA GONZALEZ
FALL 2016

A thesis
submitted in partial fulfillment
of the requirements
for a baccalaureate degree
in Biomedical Engineering
with honors in Biomedical Engineering

Reviewed and approved* by the following:

Cheng Dong
Distinguished Professor and Department Head of Biomedical Engineering
Thesis Supervisor

William Hancock
Professor of Biomedical Engineering
Honors Adviser

* Signatures are on file in the Schreyer Honors College

ABSTRACT

Conventional chemotherapeutic treatments for breast cancer produce high systemic concentrations while local concentrations in the diseased tissue are relatively low. In contrast, targeted therapeutics provide the promise of low systemic dosage, and therefore, modest or no side effects, while producing high local concentrations at the tumor. Fluorescent, 20nm diameter, calcium phosphosilicate nanoparticles (CPSNPs) synthesized in our laboratory were used as in vitro model particulate systems to evaluate targeted uptake in human breast cancer. The uptake of the CPSNPs in MDA-MB-231 breast cancer cells was analyzed to demonstrate the efficacy of the target approach using anti-CD71 as a target for the triple negative MDA-MB-231. To simulate the circulating conditions of human blood in vitro, the breast cancer cells were exposed to the CPSNPs for 30, 60, or 120 minutes under shear provided by a cone-plate viscometer placed in an incubator maintained at 37°C and 5% CO_2 to mimic the conditions of blood circulation. Flow cytometry was used to quantify the uptake of the CPSNPs, doped with Rhodamine-WT, by the cells.

In addition, commercial, fluorescent, 1 micron diameter polymeric spheres were used as a control to demonstrate the efficacy of the target approach using anti-CD71 as a target for the triple negative MDA-MB-231. The results support the in vitro anti-CD71 targeted uptake of both the CPSNPs and the microspheres by the MDA-MB-231 cells. The uptake of the anti-CD71 functionalized particles was significantly higher under both

high and low shear conditions than either the methoxy-PEG or citrate functionalized particles.

Furthermore, preliminary steps were taken to test the efficacy of docetaxel-encapsulating CPSNPs in mitigating tumor cell extravasation during metastasis. Free docetaxel concentrations as low as $1x10^{-5}$ M and $1x10^{-6}$ M were found to significantly reduce breast cancer cell extravasation across an endothelial cell monolayer, thereby demonstrating the promise of docetaxel-CPSNPs in hindering tumor cell metastasis.

TABLE OF CONTENTS

LIST OF FIGURES

LIST OF TABLES

ACKNOWLEDGEMENTS

First and foremost, I would like to thank Dr. Cheng Dong for his continuing guidance, keen thinking, and unwavering encouragement. Furthermore, my sincere thanks to Dr. James H. Adair for his critical thinking and contagious excitement for research and to my adviser Dr. William Hancock for his valuable suggestions and advice on my thesis work.

I would also like to thank Nmachi Anumba for her helpful work on the flow migration studies and Virginia Aragon Sanabria for her guidance and advice throughout my time working in the Cellular Biomechanics Laboratory.

Lastly, I especially would like to thank my family-Mario, Viviana, Lisandro, Natalia, Lorena, and Marina- for their endless love, support and encouragement.

Chapter 1

Introduction

Breast cancer is the development of malignant tumor cells in the breasts. It is the second leading cause of cancer death in women in the United States, with one in eight women developing invasive breast cancer in their lifetime[1]. Furthermore, it is estimated that over 230,000 women in the United States are diagnosed with breast cancer each year. Of these women, over 40,000 will die from the disease. Though more rare, men can be diagnosed with breast cancer, as well. Over 2,000 men are diagnosed with breast cancer and 430 of these men will die of the disease each year in the United States[2].

Breast Cancer Treatment Options

Current treatment options depend on the stage and type of breast cancer. For stages I, II, IIIA, and operable stage IIIC breast cancer, possible treatments includes breast conserving surgery, where only the tumor and surrounding tissue are removed, followed by lymph node dissection and radiation therapy. More intensive treatments at this stage include modified radical mastectomy, where a surgery is performed to remove the breast, most or all of the lymph nodes under the arm, and the lining over the chest muscles. Adjuvant therapies are often performed to lower the risk of the breast cancer recurring. These include chemotherapy, radiation therapy, hormone therapy, and monoclonal antibody therapy. For stage IIIB, inoperable stage IIIC, stage IV, and metastatic breast cancer, treatments include chemotherapy, chemotherapy followed by

breast conserving or total mastectomy surgery, clinical trials using new anticancer drugs, hormone therapy, radiation therapy, and monoclonal antibody therapy. Many of these treatment options can be used in combination to increase effectiveness of the treatment[1].

Breast Cancer Invasion and Metastasis

In the majority of cases, cancer deaths are caused by the formation of invasive, or metastatic, cancer. Metastases are secondary tumor sites in a location remote from the original site. They are formed when cells from the original neoplasm clone and detach from the site and spread through microcirculation to eventually colonize separate tissues and organs[3]. For breast cancer, the majority of metastases are adenocarcinomas derived from the mammary parenchymal epithelium, and predominantly originating from the terminal duct lobular unit[4].

The first step in breast cancer metastasis is the growth of the malignant tumor and local invasion of the surrounding extracellular matrix. The tumor grows on the epithelial side of the basement membrane and develops its own vascular supply, or angiogenesis, in the tissues of the breast, as demonstrated in Figure 1-1[5]. Once migrated through the basement membrane, the collection of tumor cells is now considered malignant cancer. Malignant clone cells travel from the initial tumor sight, through a process called intravasation, and enter blood and lymph channels to eventually reach venous circulation[6]. Tumor cells must survive a variety of barriers throughout the metastasis process, including the physical barrier of the basement membrane, chemical barriers such as changes in pH, and biological barriers such as regulatory extracellular matrix peptides[7,8].

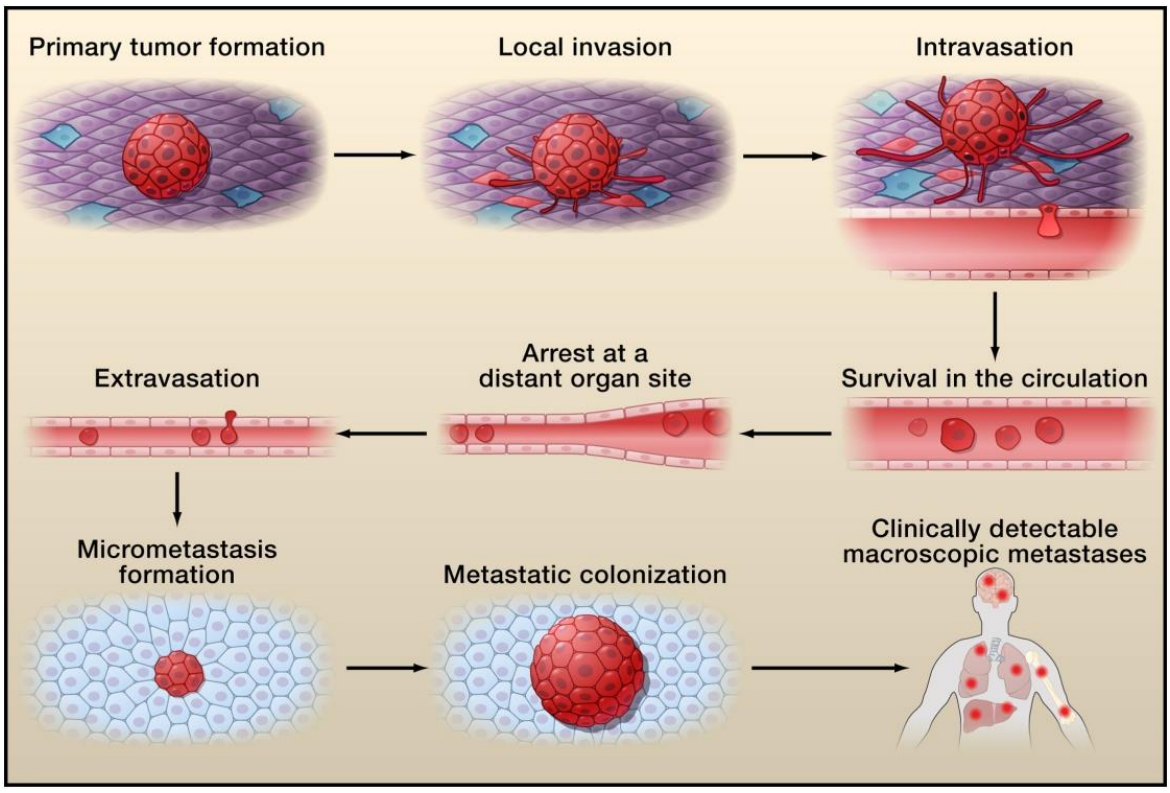

Figure 1-1. Cancer Cell Metastasis and Extravasation[5]**.** Tumor cells undergo a multistep metastasis process from initial tumor cell intravasation into venous circulation to adhesion to distant organ sites and eventual micrometastasis formation.

If the cells survive transport through the vasculature, they may arrest and adhere to the endothelium at a distant organ site. This adhesion can initiate tumor cell extravasation through the lumina of vessels and penetration of the parenchyma, thereby gaining access to the secondary site. If successful extravasation occurs, the tumor cells will attempt to form a micrometastasis and subsequently colonize local tissue[3].

The metastasis and extravasation cascade often occurs in metastatic breast cancer with the invasion of other organs, such as the lungs and brain. After intravasation into local blood circulation, malignant breast cancer cells can enter the right side of the heart and either exit

through the pulmonary artery to the lungs or cross the patent foreman ovale to enter systemic circulation.

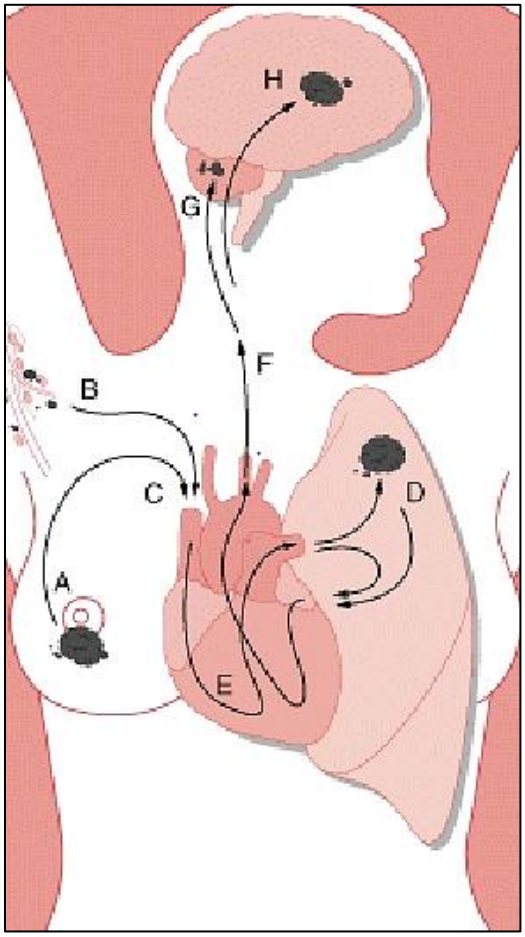

Figure 1-2. Metastatic Process of Breast Cancer to Lungs and Brain[9]. Breast cancer cells often enter systemic circulation forming metastases at distant organ sites, including the brain, bones, liver, and lungs.

The cells which enter the lungs either remain in the lungs and form pulmonary metastases or continue past the pulmonary vasculature to enter the pulmonary venous circulation. These cells can then enter the left heart to exit into systemic circulation. From there, the cells can eventually enter the cerebral circulation and arrest in brain capillaries and venules and grow within the

brain. In addition to the lungs and the brain, metastasis of breast cancer often affects other organs, including the liver and bones[9].

Effects of Mechanical Forces on Tumor Cell Metastasis

Tumor cells are exposed to dynamic flow conditions during intravasation, circulation downstream of the primary tumor site, and extravasation into secondary target sites[10]. A variety of mechanical forces originate from the extracellular matrix and surrounding tissues via adhesion receptors and mechanical loads, including interstitial forces and shear flow[11]. During cell extravasation located in the microvasculature, tumor cells are often exposed to relatively low shear forces; however, they are still affected due to changes in vascular cell function and activated cell surface receptors[10]. Furthermore, tumor cells are affected by an assortment of flow conditions, including flow patterns, level of shear, time of exposure, and composition of fluid[12]. Though both shear rate and shear stress vary throughout microcirculation, differences in shear rate, rather than shear stress, are believed to have a more significant effect, as was found during polymorpho-nuclear neutrophil-facilitated melanoma adhesion and extravasation[13].

As tumor cells are exposed to mechanical forces from their environment, they in turn, exert mechanical forces. Exposure to shear stress activates signaling pathways in tumor cells. These pathways induce tumor cell cytoskeletal reorganization and adhesive machinery[11]. Furthermore, it has been shown that shear may facilitate reinforcement of the tumor cell structure and its adhesion to the vascular wall, since shear was found to induce colon cancer cell adhesion via an Src/PI3K/FAK/Akt pathway[14].

Specifically, the capacity of tumor cells to adhere to the extracellular matrix of endothelial cells in vasculature is directly related to the ability of these cells to metastasize. A variety of cellular adhesion molecules play a part in the binding and subsequent transendothelial migration of tumor cells. In particular, VCAM-1, or Vascular Cell Adhesion Molecule 1, is an immunoglobulin-like adhesion molecule and is heavily expressed on activated endothelial cells[15]. Therefore, it is a common point of target for tumor cell binding. The integrin VLA-4 , or Very Late Antigen 4 ($\alpha_4\beta_1$, CD49d/CD29) is a counterreceptor to and has a high affinity interaction with domains 1 and 4 of VCAM-1[16]. VCAM-1 surface expression is increased in sites of inflammation and metastasis via inflammatory cytokines, such as tumor necrosis factor alpha (TNF-α)[17]. Expression of VCAM-1 on the human pulmonary microvascular endothelial cell line (HPMEC) has been confirmed under both unstimulated and TNF-α stimulated conditions with upregulated expression seen under stimulated conditions. Furthermore, the VLA-4/VCAM-1 adhesion mechanism was shown to mediate melanoma cell adhesion to the endothelium and extravasation under low shear stress, though under high shear stress, melonama adhesion and extravasation were not seen[16].

Side Effects of Chemotherapeutics and Docetaxel

Current conventional chemotherapeutics are usually systemically delivered, meaning that they circulate throughout the body in a nonspecific fashion. To address the limited pharmacological efficiency that systemic dosing provides, high dosing of chemotherapeutics is given to patients. However, these toxic compounds do not target cancer cells and attack any proliferating cells, including normal, healthy cells[18]. Due to this nonspecific targeting,

chemotherapeutics can often cause intense and harmful side effects which harm patients both physically and mentally, inhibiting their quality of life[19]. Secondary management of these associated side effects is often required to help patients cope; however, it is often insufficient to mitigate the drawbacks of the high dosing[18].

For breast cancer and other cancers, the cytotoxic drug, docetaxel (Taxotere made by Sanofi-Aventis), has emerged as a commonly-used treatment with proven clinical efficacy[20]. Docetaxel works by damaging cell growth mechanisms through the disruption of the functioning of microtubules and the inhibition of the anti-apoptotic gene Bcl2. Docetaxel also encourages the expression of the cell cycle inhibitor, p27. Through these effects, docetaxel prevents the replication and formation of cells, as well as causes existing cells to undergo apoptosis. Nevertheless, the efficacy of this treatment is coupled with little precision causing serious drug-induced side effects. The side effects of docetaxel include neuropathy, neutropenia, hypersensitivity reactions, fluid retention, asthenia, and alopecia[21]. Ironically, these side effects and treatment-associated conditions often require their own treatments. If not properly-managed, these side effects can often outweigh the potential benefits of the treatment. Though docetaxel has been proven to extend life expectancy in cancer patients above other treatments, the drug-related side effects can lead to therapy cessation, interruption or dose reduction which can compromise treatment[20].

Calcium Phosphosilicate Nanoparticles Schematic and Advantages

Calcium phosphosilicate nanoparticles (CPSNPs) are non-toxic, biodegradable vehicles that deliver chemotherapeutic drugs in lower systemic dosages, but with greater efficacy, than

conventional treatments. These particles are approximately 20 nm in diameter, are non-agglomerating, are stable at physiological pH (pH 7.4), and pose no inherent toxicity[22]. Furthermore, CPSNPs have been shown to improve the lifetime and quantum properties of encapsulated fluorescent dyes[23]. The calcium phosphosilicate core has the ability to shelter cells from the encapsulated drugs, decreasing toxicity to healthy cells and therefore, decreasing drug-related side effects. Finally, CPSNPs can be surface functionalized and/or bioconjugated to increase passive and active target specificity[24].

CPSNPs are synthesized through a double reverse-micelle procedure. The particles consist of a calcium phosphate core with silicate acting as a nucleation agent. Chemotherapeutic drugs and dyes can be encapsulated within the core for drug delivery and bioimaging functions. Furthermore, the surfaces of the CPSNPs can be functionalized for passive and selective targeting purposes[25]. A schematic of the calcium phosphosilicate nanoparticle can be found in Figure 1-3, below.

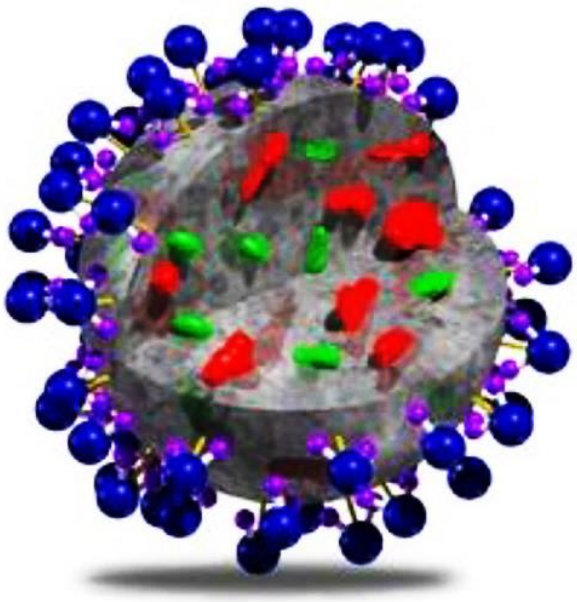

Figure 1-3. Schematic of Calcium Phosphosilicate Nanoparticle[25]. CPSNP composition includes a calcium phosphate matrix (gray), encapsulation of an active agent (green) with alternative payloads (red), and full surface functionalization (blue).

The schematic provides a depiction of the various parts of a CPSNP. The parts include a calcium phosphate matrix (gray), which encapsulates the active agent (green) with alternative payloads (red), and a full surface functionalization (blue). Examples of active agents include chemotherapeutic drugs and bioimaging agents, while surface functionalization includes citrate coatings or bioconjugated molecules.

Calcium phosphosilicate nanoparticles provide many advantages over conventional treatments. One novel feature of the particles is the pH-triggered release of the active agents. CPSNPs degrade only in low pH environments, allowing them to safely protect their encapsulated drug during systemic circulation and to protect the body from the toxic side effects caused by the drug. This also allows CPSNPs to be cleared in vivo via the hepatobiliary tract,

since they will dissolve and release their encapsulated drug only at the low pH environment of tumor cells and late-stage endolysosomes for effective clearance[26]. In addition, CPSNPs are nontoxic, since the degradation products of the particles are abundant in physiological systems and thus, are biocompatible[24].

For common systemic treatments, the maximum tolerated dose is not simply the dosage to kill the disease, but the maximum amount that can be administered without incapacitating the host[27]. By encapsulating the chemotherapeutic drug and protecting non-cancerous cells from the toxicity, the systemic dosage can be decreased while the efficacy of treatment can be increased. This allows the disproportionately high dosing to be decreased and the secondary management of associated side effects to be mitigated[18].

Active and Passive Targeting

Through surface functionalization, nanoscale drug delivery systems can make use of active and passive targeting to increase the specificity of targeting. More specific targeting to tumor sites increases efficacy of treatment and lowers the needed systemic dosage of chemotherapeutics. Passive targeting makes use of the enhanced permeability and retention (EPR) effect to increase the accumulation of nanoparticles within solid tumor sites[24].

Tumor vasculature is comprised of poorly-aligned endothelial cells with wide fenestrations. These wide gaps in the defective vasculature architecture of tumors allow for increased permeability as compared to normal, healthy endothelial tissue. Larger particles are able to permeate through the endothelial wall of tumor sites, allowing nanoparticles to have easier access to the tumor tissue than to healthy tissue. Therefore, the EPR effect allows for

altered distribution of the nanoparticles. This describes the higher concentration accumulation of nanoparticles in the tumor tissue than in plasma or other tissues[27].

Although a passive targeting approach often provides a basis for drug delivery systems, its random nature results in various limitations, including a lack of control of the drug[28]. Nevertheless, the efficacy of targeting can be further enhanced by the surface functionalization of the particles to allow for active targeting. The surface of the particles can be modified through the bioconjugation of affinity ligands, such as antibodies, peptides, and aptamers, that only bind to specific receptors on cell surfaces[27]. To ensure specific targeting, these receptors must be highly expressed on tumor cells and not on healthy cells. The targeting agents will thereby have increased targeting specificity, allowing for faster delivery and smaller systemic dosages.

Citrate, PEG and Anti-CD71 Surface Functionalization

Calcium phosphosilicate nanoparticles can be surface functionalized with citrate, polyethylene glycol (PEG), and anti-CD71, a transferrin antibody which is highly expressed on the surface of breast cancer cells. Citrate functionalized CPSNPs are used as a platform for further bioconjugation with methoxy-PEG and/or anti-CD71 antibodies. Methoxy-PEG is conjugated to citrate-terminated CPSNPs using an amide linkage between the amine termination of PEG and the carboxyl group from the citrate on the CPSNPs surface[24].

Methoxy-PEG CPSNPs can passively target tumor cells via accumulation caused by the enhance permeation and retention (EPR) effect[29]. In past studies, PEG bioconjugated CPSNPs have been shown to have increased circulation time and increased passive tumor accumulation, as compared to citrate particles[24]. PEGylation of CPSNPs has proven to be an effective passive

targeting strategy; however, interest lies in using active targeting to deliver chemotherapeutic agents to cancer cells. The ultimate goal is to have low localized concentrations of chemotherapeutics in the targeted tissue with low systemic concentrations.

To produce active targeting by the particles, PEGylated CPSNPs are further bioconjugated to express the anti-CD71 antibody by conjugating the antibody to an intermediate carboxy group from a carboxy-PEG-amine. The CD71 transferrin receptor transports iron via transferrin interactions, as needed metabolically. The CD71 receptor is prevalent on proliferating cells with high metabolic levels, such as cancerous cells, and therefore, is overexpressed on the surface of the triple negative MDA-MB-231 human breast cancer cells. Previous in vitro studies have proven the overexpression of the transferrin receptor on the surface of MDA-MB-231 human breast cancer cells, thereby demonstrating the usefulness of the anti-CD71 antibody as a targeting approach, as shown in Figure 1-4, below[24].

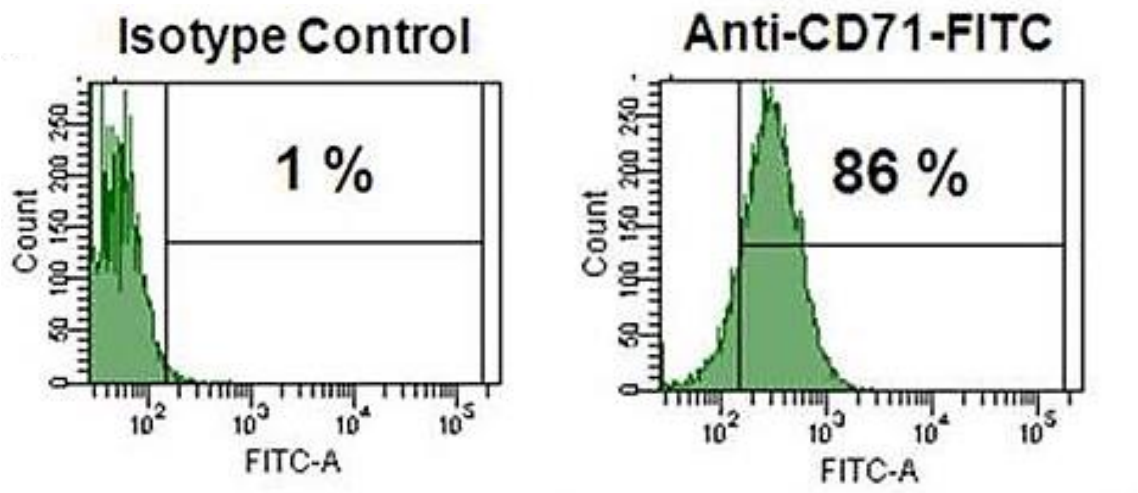

Figure 1-4. Flow Cytometry Images for Analysis of Presence of Transferrin Receptor on MDA-MB-231 Human Metastatic Breast Cancer Cells[24]. CD71 surface receptors were found to be prevalent on the surfaces of metastatic breast cancer cells, indicating their usefulness as an ideal target for CPSNPs.

Flow cytometry was used to confirm the presence of the transferrin receptor on the cells of triple negative MDA-MB-231 human breast cancer cells. The results show a significant increase in the number of cells that fluoresce at higher intensity, demonstrating that the transferrin receptor was found on nearly all cells present, making it an ideal surface target for CPSNPs[24].

Encapsulation of Docetaxel

As previously mentioned, the chemotherapeutic drug, docetaxel (Taxotere, sanofi-aventis), is commonly administered to treat locally advanced or metastatic breast cancers. Multiple issues arise when docetaxel is systemically delivered, including an increased risk of serious side effects. Furthermore, the systemic delivery leads to unpredictable variability in efficacy and toxicity between patients[21]. Due to the hydrophobicity of the chemotherapeutic, docetaxel cannot simply be administered as-is and must be formulated as a solution with the solubilizing agent, Polysorbate 80. However, Polysorbate 80 has raised concerns for its potential role in the toxicological profile of docetaxel. It has been indicated that the surfactant is not an inert vehicle, but a biologically active compound. Furthermore, Polysorbate 80 has been shown to cause severe nonimmunologic anaphylactoid reactions[30].

Encapsulation of docetaxel within nanoparticles allows the hydrophobic drug to be shielded from the hydrophilic environment before being released into a cell after endocytosis. Not only does encapsulation mitigate the harmful side effects caused by docetaxel, but also it eliminates the need for the use of Polysorbate 80. This further reduces toxicological concerns caused by systemic delivery of the drug. Furthermore, the passive and active targeting made

possible by encapsulation in CPSNPs leads to increased efficacy in the delivery of docetaxel to the tumor sites.

Previous Studies

Previous studies have shown that anti-CD71-Avidin-CPNPs were more effective at targeting MDA-MB-231 cells than either human-holotransferrin- Avidin-CPSNPs or methoxy-PEG-Avidin-CPNPs. However, the current, novel bioconjugation approach for anti-CD71 CPSNPs has demonstrated similar effectiveness at targeting human breast cancer as anti-CD71-Avidin-CPNPs without the use of an avidin-biotin noncovalent coupling approach, which may jeopardize the integrity of the anti-CD71 bioconjugates[24]

Studies were then completed to investigate the effects of bioconjugation of calcium phosphosilicate nanoparticles on the uptake of the fluorescent dye, Rhodamine-WT, by MDA-MB-231 human metastatic breast cancer cells. The fluorescence intensity of the MDA-MB-231 was measured for both static and shear conditions for the interactions between the breast cancer cells and nanoparticles. Citrate, PEG, and anti-CD71 calcium phosphosilicate nanoparticles were each tested under both static and shear conditions for 30, 60 and 120 minutes. For the cell-particle associations under static, low shear, and high shear conditions, the uptake of anti-CD71 functionalized CPSNPs was found to be slightly higher than that of either PEGylated or citrate-functionalized CPSNPs for most times. However, the CPSNPs used were laundered via centrifugation. The current study seeks to demonstrate increased targeting efficacy utilizing a double-HPLC laundering approach during post-particle synthesis. This alternative laundering method removes residual organic precursors and surfactants. The presence of these particle

precursors in the final nanoparticle solution can lead to colloidal instability and toxicity. Additionally, residual surfactant can lead to changes in the surface chemistry of the particles, thereby compromising secondary surface functionalization and bioconjugation[31].

Chapter 2

Materials and Methods

Cell Culture Protocol

Cells from the triple negative MDA-MB-231 human breast cancer line and Human Pulmonary Microvascular Endothelial Cells (HPMEC ST1.6R) were cultured in Dulbecco's Modification of Eagle's Medium (DMEM) with 10% fetal bovine serum (FBS) and 1% penicillin streptomycin (PenStrep). Cells were cultured in an incubator maintained at 37 degrees Celsius and 5% CO_2 conditions. At confluence, cells were washed with Phosphate Buffered Saline (PBS) and harvested by 0.25% trypsin/EDTA. DMEM was obtained from Corning Incorporated (Corning, NY) and FBS was obtained from Atlantic Biologicals (Flowery Branch, GA). All other materials were obtained from the Life Technologies Corporation (Grand Island, NY).

Calcium Phosphosilicate Nanoparticle Synthesis

Aqueous solutions were prepared using CO_2-free deionized water and filtered using a 0.2μm cellular acetate (CA) filter. All Rhodamine-WT solutions were vortexed to ensure complete dissolution and covered with aluminum foil to minimize light degradation.

Citrate (carboxylic acid) functionalized calcium phosphosilicate nanoparticles doped with either RhWT or docetaxel were created by a five step procedure (i-v), as demonstrated in Figure 2-1.

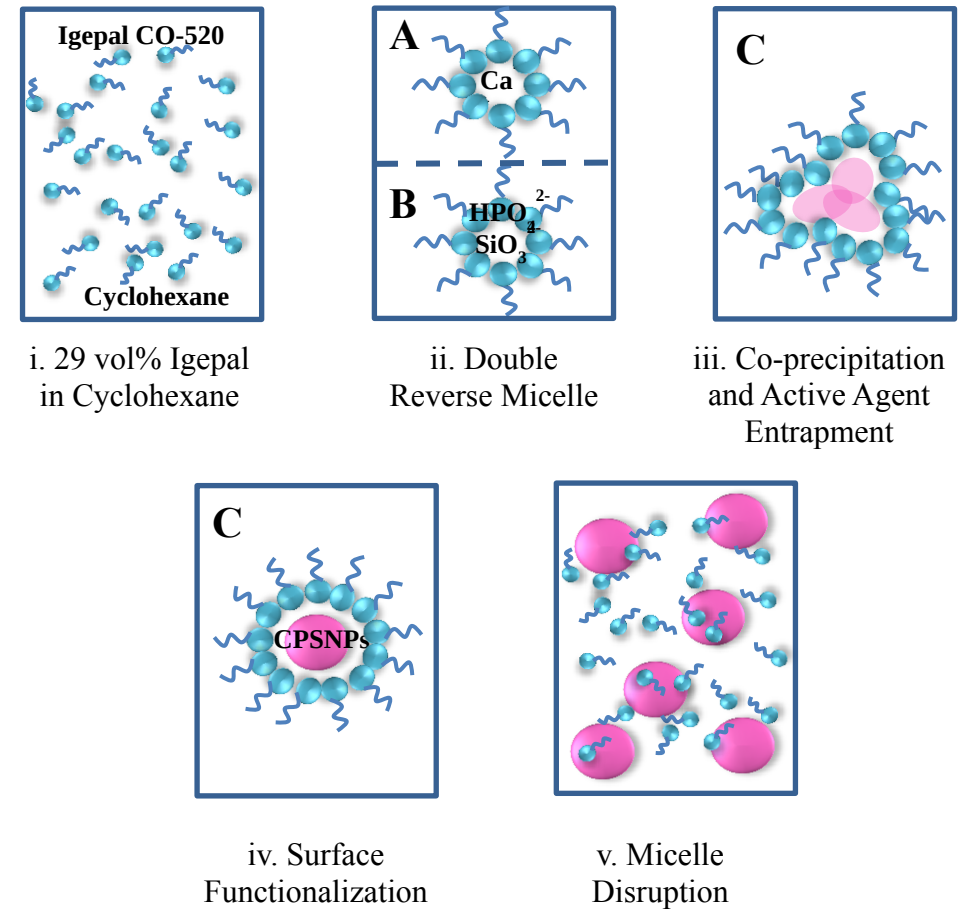

Figure 2-1. Schematic of CPSNP Synthesis. Two separate microemulsions are formed in an Igepal in cyclohexane and water solution. Afterwards, the microemulsions are combined and CPSNPs are allowed to precipitate in the micelles. Microemulsions are subsequently disrupted using an injection of pH-adjusted ethanol.

To begin the synthesis of the citrate particles, two separate microemulsions were created with a basis of 29 volume percent of Igepal® CO-520 in cyclohexane and water with a water-to-surfactant molar ratio of 4 (i). Six-hundred-fifty µL of a $CaCl_2$ ($1x10^{-2}$ M)

aqueous solution were injected into 14 mL of the 29 vol% Igepal CO-520 in cyclohexane to form microemulsion A. Immediately after, 65 μL of a Na_2HPO_4 ($6x10^{-2}$ M) aqueous solution, 65 μL of a Na_2SiO_3 ($8.2x10^{-3}$ M) aqueous solution, and 520 μL of a Rhodamine-WT ($1x10^{-1}$ M) aqueous solution were added to the other 14 mL of 29 vol% Igepal CO-520 in cyclohexane to form microemulsion B and stirred using a stir bar at 220 rpm for 15 minutes. The addition of the aqueous solutions to the Igepal CO-250 in cyclohexane creates a self-assembled reverse micelle suspension. Both microemulsions were continuously stirred using a stir bar at 220 rpm (ii).

The first microemulsion was then poured into the second microemulsion, and the micellular change was allowed to equilibrate while being stirred at a low rate for 2 minutes. During this time, the calcium phosphosilicate nanoparticles precipitated in the micelles (iii). Following the 2 minutes, 222 μL of a Na_2HCit dispersant were injected into the combined microemulsion to prevent nanoparticle agglomeration (iv). Then, the microemulsion was continuously stirred for 15 minutes at a low stir rate. Fifty mL of pH-adjusted ethanol (1 L adjusted with 300 μL of 1M KOH) were then injected to disrupt the microemulsion. The microemulsion was then stirred for 1.5 minutes at 220 rpm (v)[32].

Post-synthesis, the nanoparticles were laundered using a packed column van der Waals High Performance Liquid Chromatography (vdW-HPLC) technique to wash out cyclohexane, Igepal CO-520, and other residuals ions. For the HPLC procedure, a Waters Delta Prep 3000 HPLC System (Miford, MA) was used to pump the CPSNP solution, while a Shimadzu SPD-6A UV-visible spectrophotometric detector (Shimadzu North America) was used to measure response. A digital multimeter and ScopeView software (Radioshack, inc.) were used to plot the detector response versus time. The HPLC

procedure consisted of four stages. The last three stages (i-iii) are depicted in Figure 2-2, below[31].

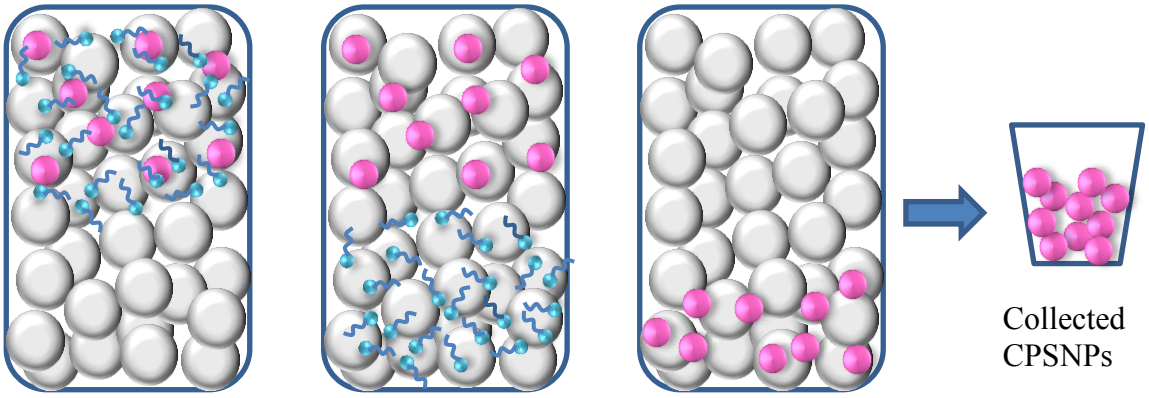

Figure 2-2. High Performance Liquid Chromatography Procedure for Washing CPSNPs. Surfactants and residual ions are removed from the nanoparticle solutions via a four step procedure: Preconditioning of the HPLC system using neat ethanol, loading of particles into the column with stationary phase spheres, washing using neat ethanol, and elution of particles using 70 vol% ethanol in water.

First, the stationary silica phase of the connecting column connected to both the HPLC pump and the spectrophotometer was preconditioned using neat ethanol. Second, the particles in the 25% cyclohexane/63% ethanol/10% igepal/2% water mobile phase were loaded into the column and deposited onto the stationary phase spheres (i). Third, neat ethanol (pH adjusted with KOH) was used to launder the particles by removing surfactant and ions (ii). Lastly, the particles were eluted out of the column and collected by using pH-adjusted, 70 vol% ethanol in water (iii). The collected particles were then diluted in a one-to-five concentration with pH-adjusted ethanol and then laundered a second time

with vdW-HPLC to remove cytotoxic residual Igepal. Citrate-CPSNPSs were stored at 4°C with light protection[31].

The previous citrate-functionalized product was then filtered through a 0.2 µm regenerated cellulose filter and stirred on a stir plate at 550 rpm. It was then activated using 1 mL of N-(3-Dimethylaminopropyl)-N′-ethylcarbodiimide hydrochloride (EDC, 2 mg/mL) and stirred for 5 minutes. One mL of sulfo-N-hydroxysuccinimide (sulfo-NHS, 1.5 mg/mL) was then reacted with the citrate particles and stirred for 5 minutes to form a semistable intermediate. Afterwards, a methoxy-PEG-amine solution was added and the reaction was allowed to occur for 15 hours at 50 degrees Celsius and 550 rpm. If the desired product was a PEGylated CPSNP, the previously created sample was washed and filtered through an Amicon® Ultra-4 centrifuge filtration unit (30kD, EMD Millipore, Billerica, MA) via centrifugation at 7000 g for 2 minutes. The filtered solution was then filtered again at 7000 g for 2 minutes to recover CPSNPs that passed through the filter during the first filtration. The methoxy-PEGylated CPSNPs were dried using argon gas and stored at 4°C with protection from light[32].

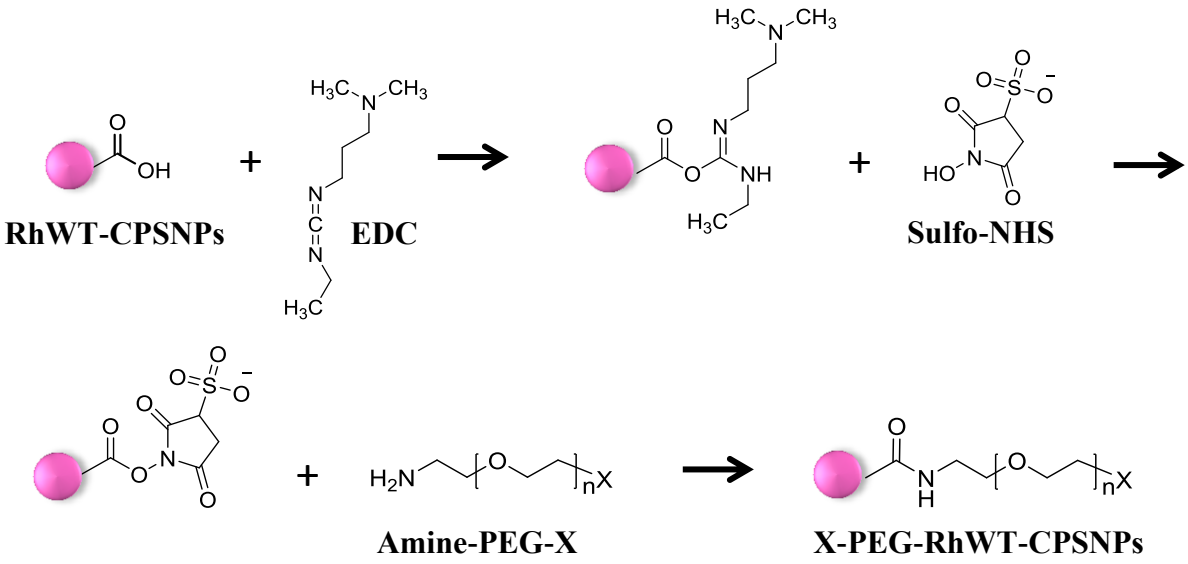

Figure 2-3. PEGylation of RhWT-CPSNPs. RhWT-CPSNPs are PEGylated by activation with EDC, reaction with Sulfo-NHS to form a semistable intermediate, and reaction with methoxy-PEG-amine to form the final methoxy-PEG-RhWT-CPSNPs.

Calcium Phosphosilicate Nanoparticle Bioconjugation

To create anti-CD71 functionalized particles, the previous steps were repeated up to the addition of the Sulfo-NHS solution. After this, a mixture of CO_2-free water and the anti-CD71 antibodies (0.833 mL, 0.06 mg/mL) were added to the previously PEGylated CPSNPs to form the final anti-CD71 functionalized CPSNPs. The particles were then stirred for 3 hours before being stored for 6 hours at 4 degrees Celsius. After a minimum of 6 hours, the particles were then washed and filtered using HPLC and dried using Argon gas. A full schematic of the chemical synthesis of the antibody bioconjugated CPSNPs can be seen in Figure 2-4.

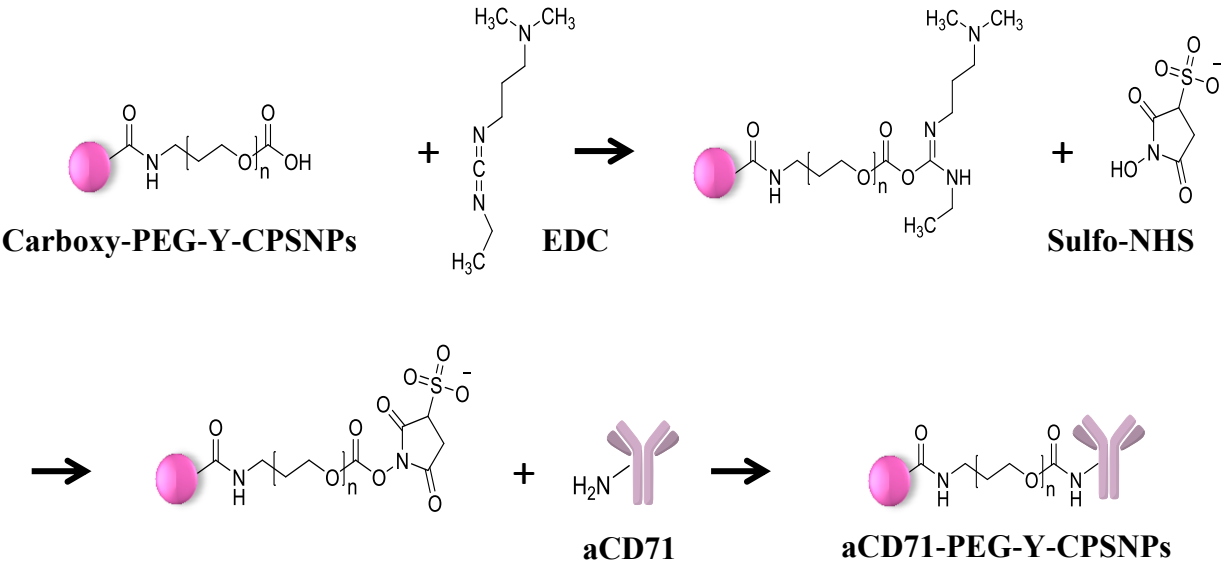

Y = RhWT, Docetaxel

Figure 2-4. Bioconjugation of CPSNPs with Anti-CD71. Carboxy-PEG-RhWT-CPSNPs are bioconjugated by activation with EDC, reaction with Sulfo-NHS to form a semistable intermediate, and reaction with an anti-CD71 solution to form the final aCD71-PEG-RhWT-CPSNPs.

Before use, all of the CPSNP samples were dried with Argon gas and resuspended in DPBS, maintaining the desired RhWT concentration[32]. All RhWT-encapsulated particles for this thesis were prepared by Xiaomeng Tang from Dr. James H. Adair's material science and biomedical engineering laboratory at the Pennsylvania State University. Citrate particles were from batch XT8-72, methoxy-PEGylated particles were from batch X9-6-1, and anti-CD71 particles were from batch XT9-6-25. Xiaomeng Tang's notebooks are stored in the lab of Dr. Adair.

Shear Experiment Preparation and the Cone-Plate Viscometer

To simulate the associations of particles and cells in blood circulation, shear experiments were conducted by exposing MDA-MB-231 human metastatic breast cancer cells to the CPSNPs on a cone-plate viscometer, an instrument with a 1 degree rotating cone. Once confluent, the cells were harvested using trypsin/EDTA and allowed to recover their surface proteins on a rocker for 30 minutes in 37 degree Celsius and 5% CO_2 conditions. A volume of cells corresponding to 500,000 cells was taken from the sample and centrifuged for 5 minutes at 1500 rpm. They were then resuspended in a volume of medium corresponding to a RhWT concentration of 1.45×10^{-6} M for the particles, so that the final total volume of cells and particles would be 1 mL.

The cell volume was then placed on a HAAKE RotoVisco 1 cone-plate viscometer (Rheology Solutions, Victoria, Australia) that was kept in an incubator maintained at 37 degrees Celsius and 5% CO_2 conditions. The cone-plate viscometer consists of a 1 degree free cone rotating at a constant velocity gradient. Figure 2-5 is a depiction of the cone-plate viscometer set-up.

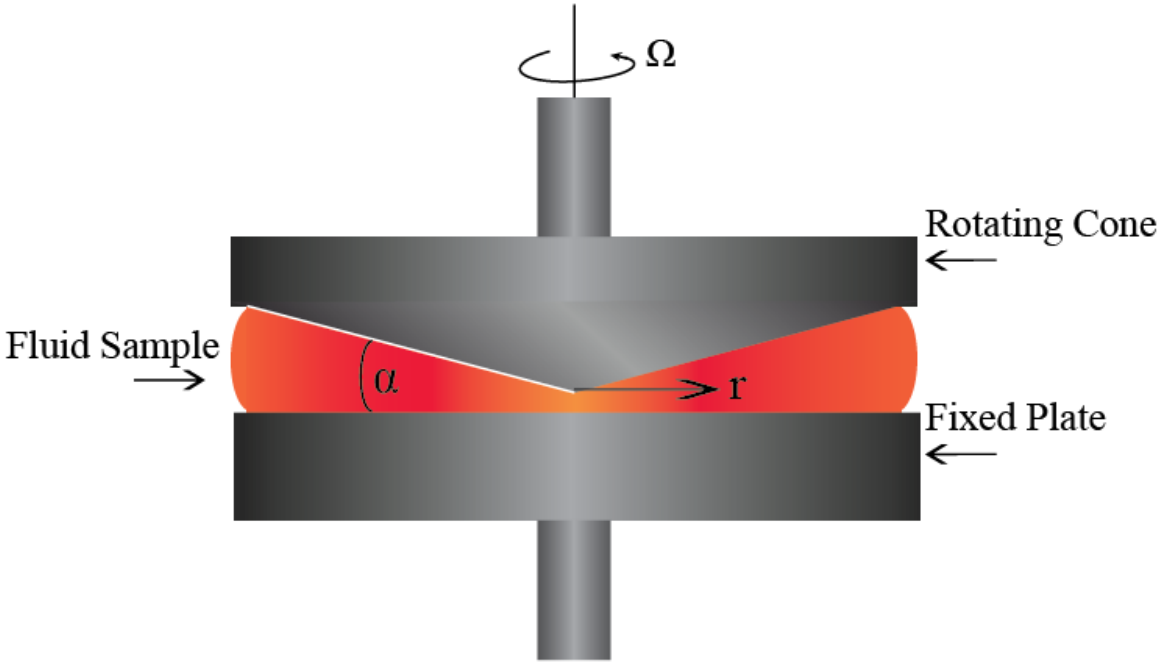

Figure 2-5. Depiction of Cone-Plate Viscometer. This instrumentation consists of a 1-degree rotating cone creating a uniform shear field across the entire fluid sample.

Shear rates were maintained at either 62.5 sec^{-1} or 200 sec^{-1} for low or high shear experiments, respectively, to mimic the shear conditions of blood flow[33]. The shear rate of the cone-plate viscometer is set by the angular frequency of the rotating cone. The shear rate profile is determined by the following equation:

$$\dot{\gamma} = \frac{2\pi\Omega}{60\alpha}$$

, where $\dot{\gamma}$ is shear rate in sec^{-1}, Ω is the cone rotational rate in revolutions per minute, and α is the angle between the cone and plate. Since the angle of the cone-plate is maintained at 1 degree, the shear rate has a linear relationship with the rotational rate of the cone. Therefore, the shear rate was directly controlled by the speed of the cone[34]. Furthermore,

the viscometer design allows a uniform shear field to be applied to the entire fluid sample[35,36].

At each time point (30, 60, and 120 minutes), two-100 μL volume samples were collected and centrifuged for 5 minutes at 1500 rpm. Following centrifugation, the cells were resuspended in 2.5 volume % formaldehyde in DPBS and allowed to fix for 10 minutes at 4 degrees Celsius. After the ten minutes, cells were resuspended in 200 μL DPBS. The above steps for washing and fixing were also taken for a sample which was not exposed to the CPSNPs doped with Rhodamine-WT, in order to serve as a control. All cells were then ready to be analyzed using flow cytometry[29].

Flow Cytometry and Fluorescent Microscopy Analysis

To quantify the uptake of the CPSNPs doped with Rhodamine-WT (RhWT-CPSNPs) by the cells, a Guava PCA flow cytometer was used (Guava Technologies, Inc., Hayward, CA). The cytometer measured the fluorescence intensity of the cells treated with RhWT-CPSNPs, in order to indicate the extent to which the particles were taken up by the cells. The mean fluorescence intensity was determined using Cytosoft Guava Express software. Control samples were analyzed, as well, from the original cell samples that were not exposed to the CPSNPs[37].

After flow cytometry analysis, the cells were imaged using a NIKON TE-2000 microscope (Nikon Instruments Inc., Melville, NY) with a 10X or 20X objective lens and the EXFO X-Cite 120 Fluorescence Illumination System (Excelitas, Quebec, Quebec).

Conjugation Technique Analysis Using Polystyrene Microspheres

Commercial, fluorescent, 1 micron diameter polymeric spheres were used to serve as a control for the efficacy of the target approach used while synthesizing the CPSNPs. The preceding steps were repeated using Nile-red polystyrene microspheres obtained commercially (Molecular Probes, inc., Eugene, Oregon). Similarly to the citrate-RhWT CPSNPS, the surfaces of these microspheres were carboxylate-terminated ($-COO^-$) and were also surface functionalized with polyethylene glycol and the anti-CD71 antibody, using a bioconjugation technique slightly different to the previously detailed procedure. After the previous steps for PEGylation detailed on page 21 above, an aqueous solution of 1mL of EDC was added dropwise to 10 mL of the PEGylated microspheres and stirred for 5 minutes. One mL of an aqueous solution of sulfo-NHS was then added dropwise and stirred for an additional 5 minutes. Afterwards, 0.833 mL of a pre-thawed anti-CD71 antibody aqueous solution was added and stirred for 3 hours. The resulting suspension was stored at 4°C for 6 hours and laundered using centrifugal filtration, since HPLC could not be used due to the large, 1 micron diameter of the beads. Sample concentrations for carboxy-terminated, PEGylated, and anti-CD71 functionalized microspheres were maintained at 3.9×10^7 particles/mL in DPBS[32]. All PEGylated and bioconjugated microspheres for this thesis were surface functionalized and prepared by Xiaomeng Tang. Methoxy-PEGylated microspheres were from batch XT7-92-2 and anti-CD71 microspheres were from batch XT7-92-4. Xiaomeng Tang's notebooks are stored in the lab of Dr. Adair.

Shear experiments were conducted using the previously mentioned protocol. The MDA-MB-231 human breast cancer cells were exposed to the microspheres for 30, 60, or 120 minutes on a cone-plate viscometer placed in an incubator maintained at 37 °C and 5% CO_2. Shear rates of 62.5 sec^{-1} and 200 sec^{-1} were used to simulate the high and low shear conditions of human blood circulation. They were then fixed with 2.5 volume % paraformaldehyde and analyzed via flow cytometry and fluorescent microscopy.

MTS Cell Proliferation Assay

To test the effects of free docetaxel on MDA-MB-231 human breast cancer cells, an MTS tetrazolium assay (CellTiter 96® AQueous One Solution Cell Proliferation Assay, Promega Corporation, Madison, WI) was performed for varying concentrations of free docetaxel. The tumor cells were exposed to either no treatment (consisting of DMEM media with 10% FBS), vehicle (1:10 dilution of DPBS in DMEM media), $1x10^{-5}$ M, $1x10^{-6}$ M, $1x10^{-7}$ M, $1x10^{-8}$ M, $1x10^{-9}$ M, $1x10^{-10}$ M, $1x10^{-11}$ M, or $1x10^{-12}$ M concentrations of free docetaxel. The free docetaxel was dissolved in 13% ethanol in DPBS. After 48 hours of incubation, 20 µl of MTS reagent [tetrazolium compound (3-(4,5-dimethylthiazol-2-yl)-5-(3-carboxymethoxyphenyl)-2-(4-sulfophenyl)-2H-tetrazolium, inner salt; MTS) and an electron coupling reagent (phenazine ethosulfate; PES)] was added to each sample and incubated. After 3 hours, absorbance was measured at 490 nm using an optical transparent 96-well plate using a Thermo Labsystems Multiskan Microplate Reader (Thermo Scientific, Rockford, IL). Absorbance values were normalized to the vehicle to quantify the proliferation levels.

Immunostaining Cells for Antibody Testing

Once confluent, MDA-MB-231 human breast cancer cells were harvested using trypsin/EDTA and allowed to recover their surface proteins on a rocker for 30 minutes in 37 degree Celsius and 5% CO_2 conditions. Cells were diluted to a concentration of 750,000 cells per mL, and a volume of 100 μL of this sample was centrifuged for 3 minutes at 1500 rpm. Supernatant was decanted and cells were then resuspended in a volume 100 μL of PBS and 1% BSA. Mouse IgG anti-human monoclonal antibodies (mAbs) against $\alpha_4\beta_1$ (anti-CD49d/CD29) (R&D Systems, Minneapolis, MN) were added and the cells were incubated on a rocker for 1 hour on ice. Cells were then centrifuged and resuspended in 500 μL of PBS and 1% BSA and washed three times. Alexa Fluor 546 goat, anti-mouse secondary antibody was added, and cells were incubated on a rocker for 1 hour on ice. Cells were then centrifuged and resuspended in 500 μL of PBS and 1% BSA and washed three times[38]. After being resuspended in 300 μL of PBS and 1% BSA, cells were ready to be run through the flow cytometer for analysis.

Flow Migration Studies

An in vitro flow migration device, consisting of a modified chemotactic Boyden chamber assay with 48-wells, was used to analyze the migration of the breast cancer cells through an endothelial cell monolayer. As depicted in Figure 2-6, the chamber consists of two polycarbonate plates separated by a 0.02-inch thick silicon gasket (PharmElast, SF Medical, Hudson, MA). The center of the gasket is cut with a 7 cm x 2 cm hole which forms the opening of the flow field. Beneath the gasket is a sterilized

polyvinylprrolidone-free polycarbonate filter with an 8 μm pore size (Neuro Probe, Gaithersburg, MD). A monolayer of HPMEC cells was grown to confluence on the center of the filter and was coated with a 30μg/ml concentration of fibronectin. Before use, the bottom side of the filter was scraped to remove any unwanted endothelial cell growth[39].

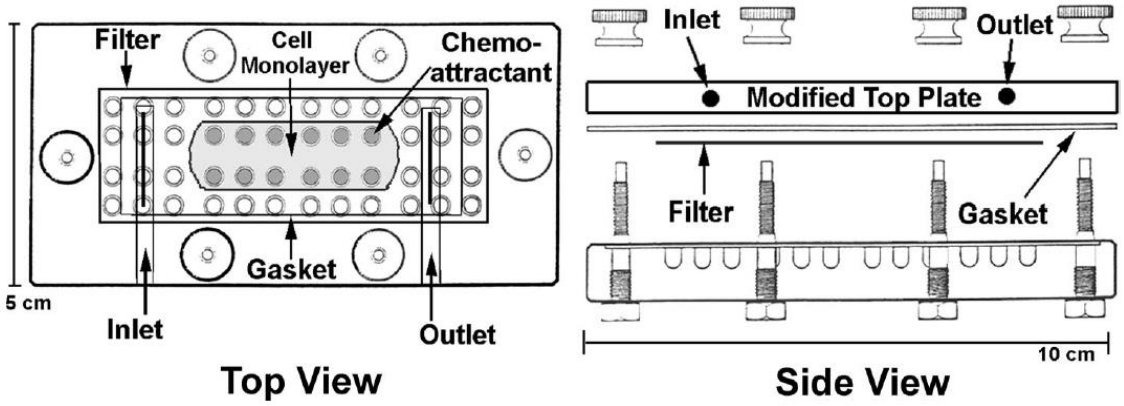

Figure 2-6. Top and Side Views of the Chemotactic Flow Migration Chamber[40]. This apparatus consists of a modified chemotactic boyden chamber assay with two polycarbonate plates separated by a silicon gasket. Beneath the gasket is a porous polycarbonate filter with an endothelial monolayer coated with fibronectin.

Within the wells of the bottom polycarbonate plate, the center twelve wells were filled with a soluble collagen IV solution of 100 μg/ml 1 w/v% BSA/DMEM to serve as a chemoattractant, and the remaining wells were then filled with 1 w/v% BSA/DMEM. The filter with the endothelial monolayer was then placed on top of the polycarbonate plate with the monolayer centered over the collagen wells. The silicon gasket and the top polycarbonate plate were then added, and the three chambers were placed within an incubator maintained at 37°C.

MDA-MB-231 breast cancer cells totaling in 6 million cells (2 million cells per each of the 3 chambers) were resuspended in a 1 w/v % BSA/DMEM solution and

circulated through the chambers, as demonstrated in Figure 2-7, at a desired flow rate for 4 hours. For the low shear experiments, a corresponding flow rate of 75 sec^{-1} was used, while a flow rate of 200 sec^{-1} was used for high shear experiments. The wall shear stress is related to the volumetric flow rate by the following equation:

$$\tau_w = 6\mu Q/wh^2,$$

where τ_w is the shear stress of the wall, μ is the fluid viscosity, Q is the volumetric flow rate, w is the width of the flow field and h is the height. Since the wall height, fluid viscosity, and width of the flow field were maintained at constant values, the shear stress could be set by the volumetric flow rate[40]. For a low shear rate of 75 sec^{-1}, the flow rate was set to 3 mL/min. For a high shear rate of 200 sec^{-1}, the flow rate was set to 8 mL/min. It should be noted that the low shear rate was a higher value from the previous cone-plate viscometer experiments, since the volumetric flow rates could not be set to intermediate values between integers.

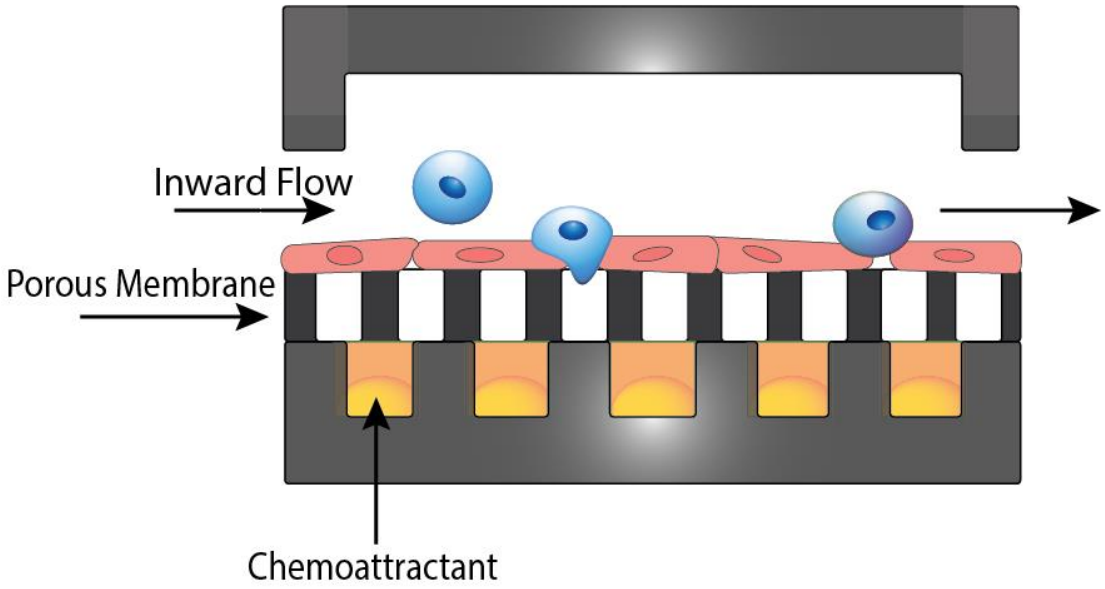

Figure 2-7. Tumor Cell Circulation and Migration in Chemotactic Flow Chamber. The flow migration chamber allows for the simulation of the movement of particles and tumor cells across a flow field and subsequent tumor cell transendothelial migration under varying flow conditions.

After the 4 hours, the filters are removed from the chambers, the HPMEC cells were scratched off, and the filters were stained with HEMA-3 (Fischer Scientific, Pittsburgh, PA). The bottom sides of the filters, which had been facing the collagen IV wells, were imaged[41]. Five images were taken using a NIKON TE-2000 microscope at different locations on each of the three filters and the cells were counted for each of the images and averaged to determine the number of migrated cells per square mm.

Statistical Analysis

The flow cytometer results from viscometer studies testing RhWT-CPSNP and Nile-red polystyrene microsphere associations were analyzed using two-tailed, unequal variance, un-paired t-tests to evaluate significant differences between shear rates. Additionally, the flow cytometry results were analyzed using one-way ANOVA for analysis between surface functionalization types.

The MTS assay results were analyzed using a one-way ANOVA to determine significant differences between absorbance values. The flow migration results were first analyzed using a one-way ANOVA and Tukey's method for multiple comparisons between all samples to evaluate differences between cell migration numbers. A p-value of less than 0.05 indicated statistically significant differences between all samples.

Chapter 3

Results of Fluorescent Polystyrene Microsphere Experiments

The following results show the flow cytometer data from the microsphere-cell association studies using carboxy-terminated, methoxy-PEGylated, and anti-CD71 microspheres encapsulated with RhWT under low and high shear conditions. The mean fluorescence intensity displayed in the graphs, which directly reflects associations with the microspheres, was determined using the GuavaExpress program. Error bars on all graphs indicate standard error for $n \geq 4$. * Above graphs indicates a p value of less than 0.05 and ** above graphs indicates a p-value of less than 0.01.

Results of Carboxy-Terminated Microsphere-Cell Associations

The results of the viscometer experiments completed for carboxy-terminated functionalized polystyrene microspheres under both high and low shear conditions for 30, 60, and 120 minutes are shown in Figure 3-1, below. The average fluorescence intensity values for carboxy-terminated polystyrene microspheres were collected after low (62.5 sec^{-1}) and high (200 sec^{-1}) shear rate exposure from the cone-plate viscometer.

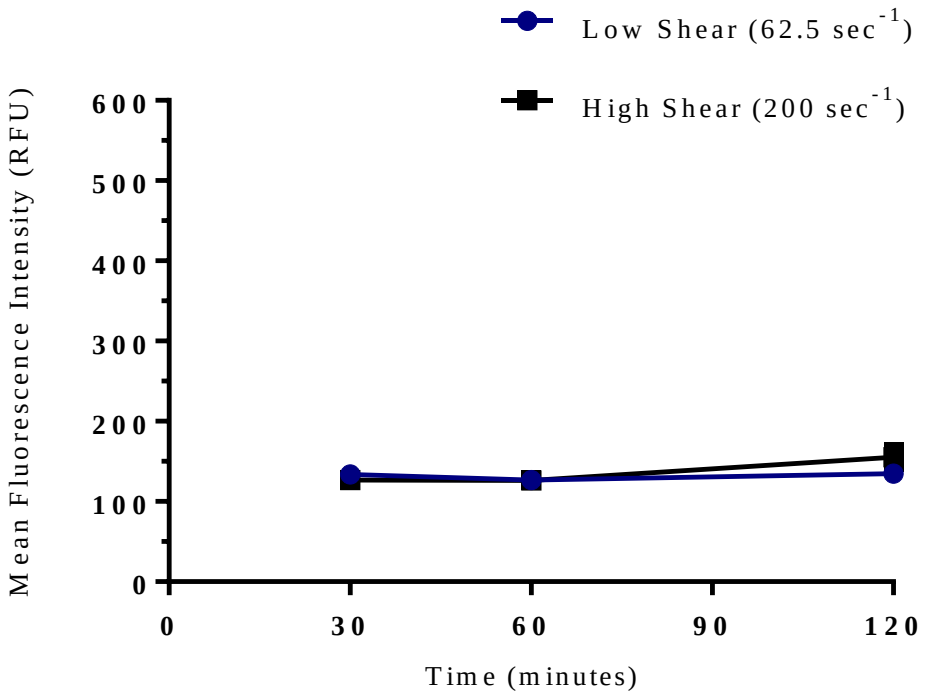

Figure 3-1. Uptake of Fluorescent, Carboxy-Terminated Microspheres after Low and High Shear Exposure. The mean fluorescence intensity of carboxy-terminated microspheres was measured after 30, 60, and 120 minutes of shear exposure. There was no significant difference seen between low shear and high shear conditions at any time point. Values are mean ± S.E.M. for $N \geq 4$.

Carboxy-terminated microspheres showed no significant differences with respect to cell associations between shear rates at any time.

Results of Methoxy-PEGylated Microsphere-Cell Associations

The results of the viscometer experiments completed for methoxy-PEG functionalized polystyrene microspheres under both high and low shear conditions for 30, 60, and 120 minutes are shown in Figure 3-2, below. The average fluorescence intensity values for

methoxy-PEG polystyrene microspheres were collected after low (62.5 sec^{-1}) and high (200 sec^{-1}) shear rate exposure from the cone-plate viscometer.

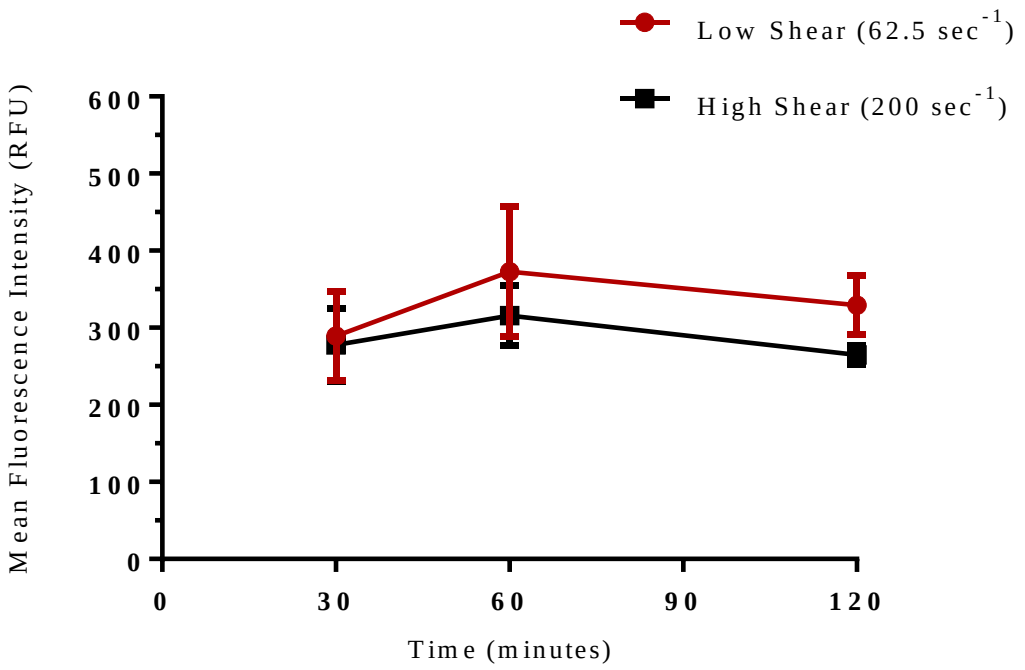

Figure 3- 2. Uptake of Fluorescent, Methoxy-PEGylated Microspheres after Low and High Shear Exposure. The mean fluorescence intensity of methoxy-PEGylated microspheres was measured after 30, 60, and 120 minutes of shear exposure. There was no significant difference seen between low shear and high shear conditions at any time point. Values are mean ± S.E.M. for $N \geq 4$.

Similar to carboxy-terminated particles, methoxy-PEG microspheres showed no significant differences at any time points between associations of differing shear rates.

Results of Anti-CD71 Microsphere-Cell Associations

The results of the viscometer experiments completed for anti-CD71 bioconjugated polystyrene microspheres under both high and low shear conditions for 30, 60, and 120 minutes are shown in Figure 3-3, below. The average fluorescence intensity values for anti-CD71 polystyrene microspheres were collected after low (62.5 sec^{-1}) and high (200 sec^{-1}) shear rate exposure from the cone-plate viscometer.

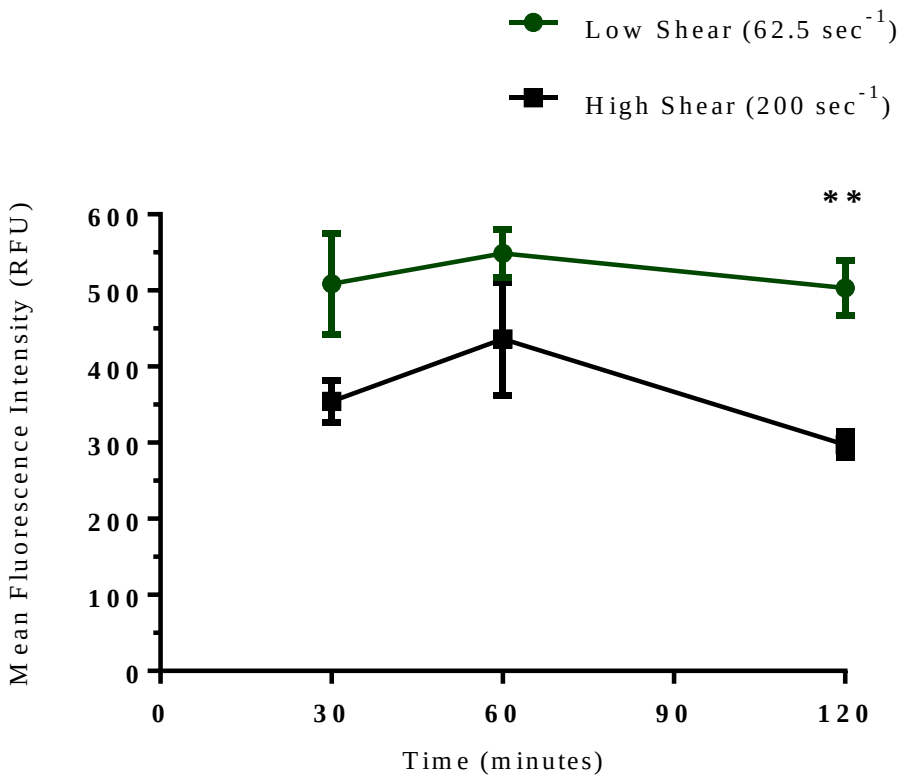

Figure 3- 3. Uptake of Fluorescent, Anti-CD71 Bioconjugated Microspheres after Low and High Shear Exposure. The mean fluorescence intensity of anti-CD71 microspheres was measured after 30, 60, and 120 minutes of shear exposure. Associations under low shear conditions were significantly higher than under high shear conditions only at 120 minutes ($p = 0.001$). **$P < 0.01$ compared with fluorescence of differing shear rate. Values are mean ± S.E.M. for $N \geq 4$.

Anti-CD71 microspheres showed significantly higher uptake under low shear conditions than under high shear conditions at 120 minutes ($p = 0.001$).

Results of Low Shear Microsphere-Cell Associations

A comparison of the results from experiments conducted on all three microsphere types (carboxy-terminated, methoxy-PEG, and anti-CD71) under low shear conditions for 30, 60, and 120 minutes are shown in Figure 3-4. The average fluorescence intensity values for all three microsphere types were collected after low (62.5 sec^{-1}) shear rate exposure from the cone-plate viscometer.

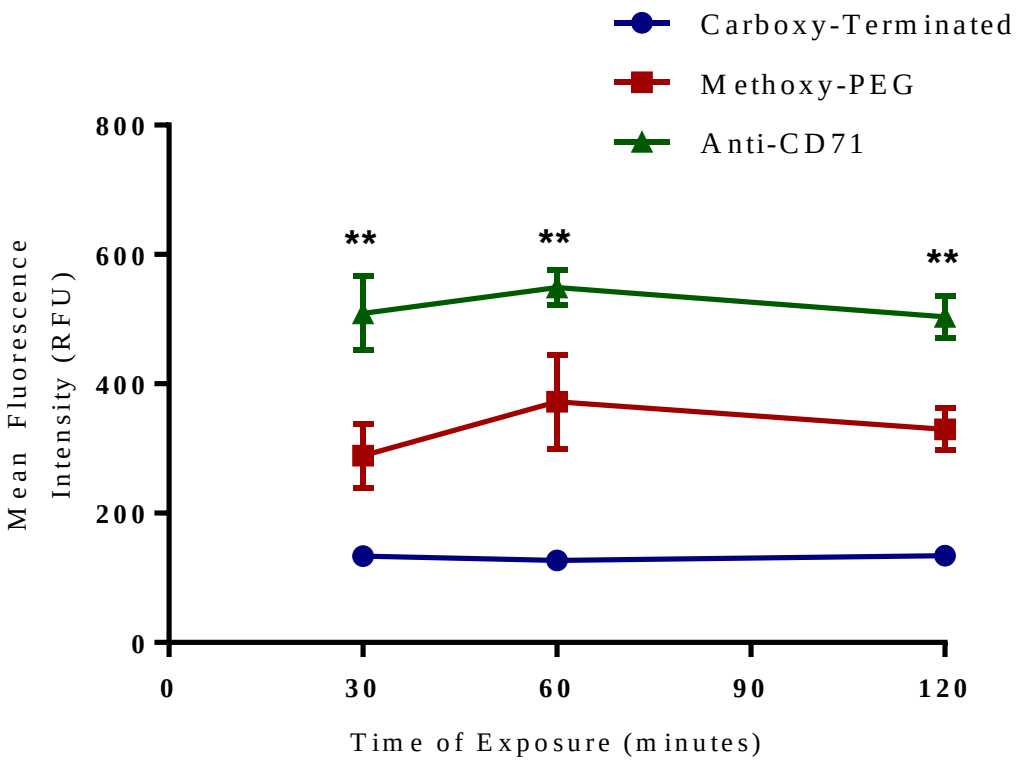

Figure 3- 4. Uptake of Fluorescent Microspheres after Low Shear Exposure. The mean fluorescence intensities of carboxy-terminated, PEG, and anti-CD71 microspheres were measured after 30, 60, and 120 minutes of low shear exposure. Anti-CD71 microspheres showed significantly higher associations than citrate and methoxy-PEG microspheres for all three time points ($p = 0.001, 0.001, 0.001$). **$P < 0.01$ for anti-CD71 particles compared with fluorescence of carboxy-terminated and PEG microspheres. Values are mean ± S.E.M. for $N \geq 4$.

Anti-CD71 microspheres showed significantly higher associations than carboxy-terminated and methoxy-PEG microspheres at 30 minutes ($p = 0.001$), 60 minutes ($p = 0.001$), and 120 minutes ($p = 0.001$). Methoxy-PEGylated microspheres also showed significantly higher uptake than carboxy-terminated microspheres at 120 minutes ($p = 0.01$). For each particle type, differences between uptake at 30, 60, and 120 minutes was

analyzed; however, no significant differences were found, indicating that the maximum associations were reached at an earlier time point.

Results of High Shear Microsphere-Cell Associations

A comparison of the results from experiments conducted on all three microsphere types (carboxy-terminated, methoxy-PEG, and anti-CD71) under high shear conditions for 30, 60, and 120 minutes are shown in Figure 3-5. The average fluorescence intensity values for all three microsphere types were collected after high (200 sec^{-1}) shear rate exposure from the cone-plate viscometer.

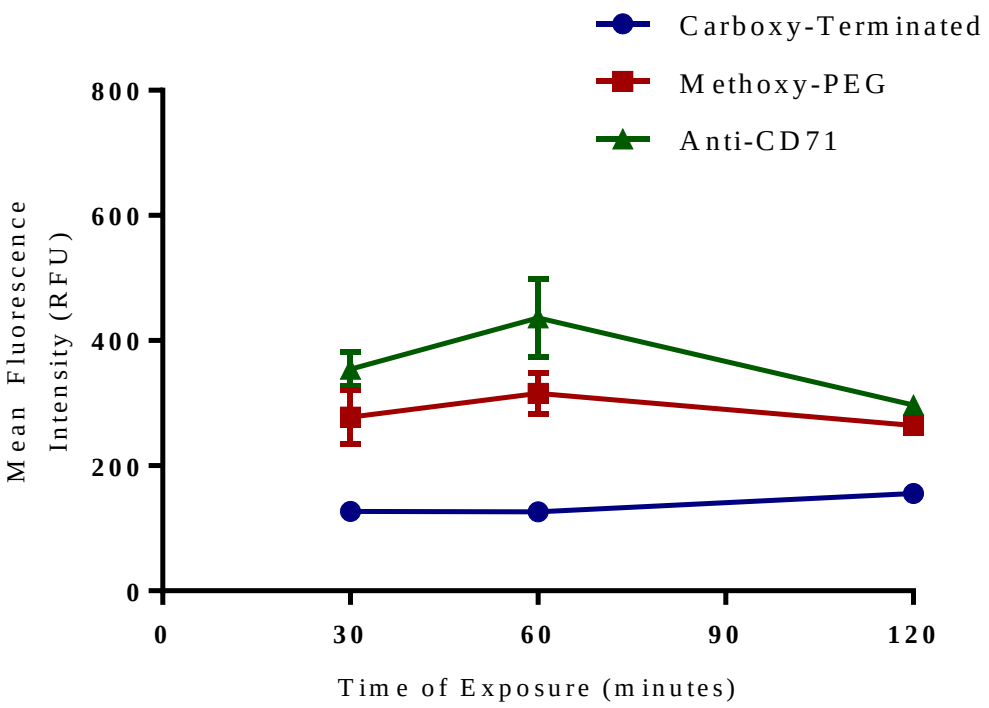

Figure 3- 5. Uptake of Fluorescent Microspheres after High Shear Exposure. The mean fluorescence intensities of carboxy-terminated, PEG, and anti-CD71 microspheres were measured after 30, 60, and 120 minutes of high shear exposure. No significant

differences in associations between anti-CD71 and PEG microspheres were seen at any time point. Values are mean ± S.E.M. for $N \geq 4$.

Anti-CD71 and methoxy-PEG microspheres showed significantly higher associations than carboxy-terminated microspheres at 30, 60, and 120 minutes ($p = 0.001, 0.001, 0.001$). However, anti-CD71 microspheres did not show significantly higher uptake than methoxy-PEG microspheres at any time point. Furthermore, anti-CD71 microspheres appear to peak at 60 minutes and then decrease in mean fluorescence intensity at 120 minutes, suggesting a decrease in microsphere-cell associations. For each particle type, differences between uptake at 30, 60, and 120 minutes was analyzed; however, no significant differences were found, indicating that the maximum associations were reached at an earlier time point.

Chapter 4

Results of Rhodamine-WT-Encapsulated CPSNP Experiments

The following results show the flow cytometer data from the particle-cell association studies using citrate, methoxy-PEG, and anti-CD71 CPSNPs encapsulated with RhWT under low and high shear conditions. The mean fluorescence intensity displayed in the graphs, which directly reflects uptake of the CPSNPs, was determined using the GuavaExpress program. Error bars on all graphs indicate standard error for n=6. * Above graphs indicates a p value of less than 0.05 and ** above graphs indicates a p-value of less than 0.01.

Results of Citrate RhWT Particle-Cell Associations

The results of the viscometer experiments completed for RhWT-encapsulated citrate CPSNPs under both high and low shear conditions for 30, 60, and 120 minutes are shown in Figure 4-1, below. The average fluorescence intensity values for citrate CPSNPs were collected after low (62.5 sec^{-1}) and high (200 sec^{-1}) shear rate exposure from the cone-plate viscometer.

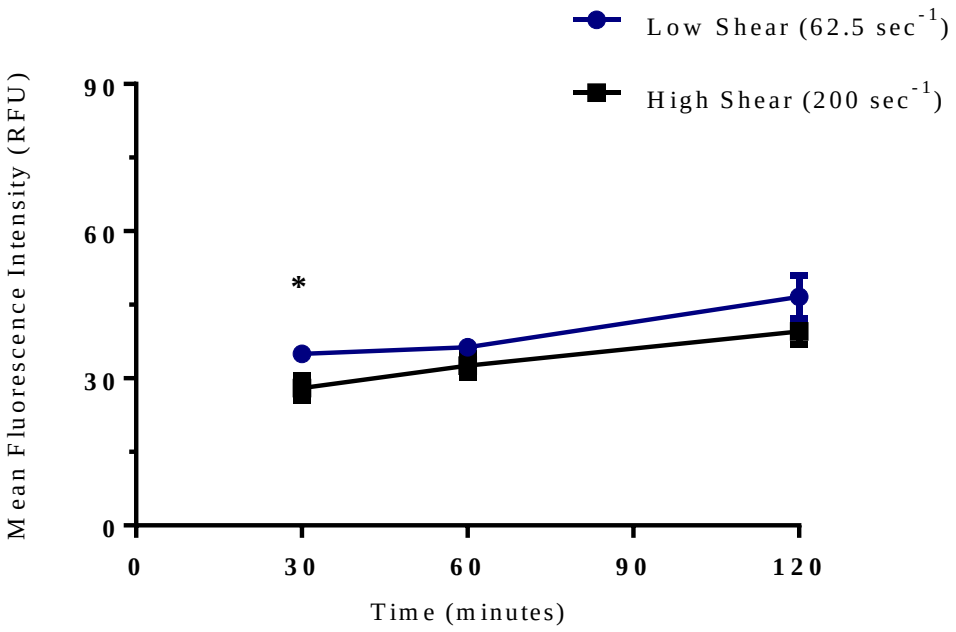

Figure 4- 1. Uptake of Citrate-Functionalized CPSNPs after Low and High Shear Exposure. The mean fluorescence intensity of citrate particles was measured after 30, 60, and 120 minutes of shear exposure. Associations under low shear conditions were significantly higher than under high shear conditions for 30 minutes only ($p = 0.04$). *$P < 0.05$ compared with fluorescence of differing shear rate. Values are mean ± S.E.M. for $N \geq 6$.

Citrate particles showed significantly higher associations under low shear rates only at 30 minutes ($p = 0.04$). No significant differences were seen between shear rates at 60 or 120 minutes.

Results of Methoxy-PEGylated RhWT Particle-Cell Associations

The results of the viscometer experiments completed for methoxy-PEG functionalized RhWT particles under both high and low shear conditions for 30, 60, and 120 minutes are shown in Figure 4-2 , below. The average fluorescence intensity values

for methoxy-PEG CPSNPs were collected after low (62.5 sec^{-1}) and high (200 sec^{-1}) shear rate exposure from the cone-plate viscometer.

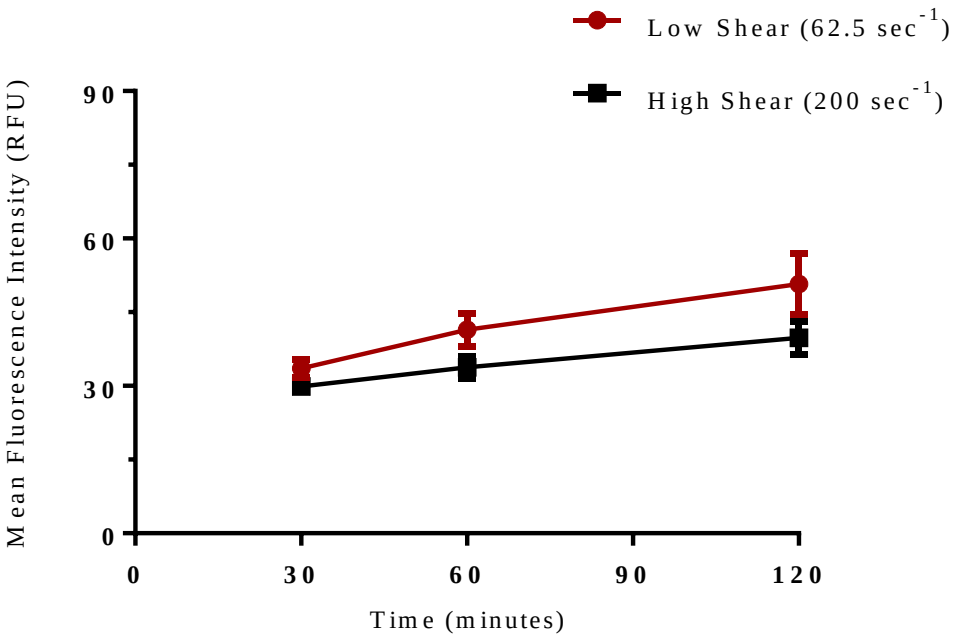

Figure 4- 2. Uptake of Methoxy-PEGylated CPSNPs after Low and High Shear Exposure. The mean fluorescence intensity of citrate particles was measured after 30, 60, and 120 minutes of shear exposure. No significant differences were seen between associations under differing shear conditions at any time point. Values are mean ± S.E.M. for $N \geq 6$.

Methoxy-PEG particles showed no significant difference at any time points between associations of differing shear rates.

Results of Anti-CD71 RhWT Particle-Cell Associations

The results of the viscometer experiments completed for anti-CD71 functionalized RhWT particles under both high and low shear conditions for 30, 60, and 120 minutes are shown in Figure 4-3, below. The average fluorescence intensity values for anti-CD71 CPSNPs were collected after low (62.5 sec^{-1}) and high (200 sec^{-1}) shear rate exposure from the cone-plate viscometer.

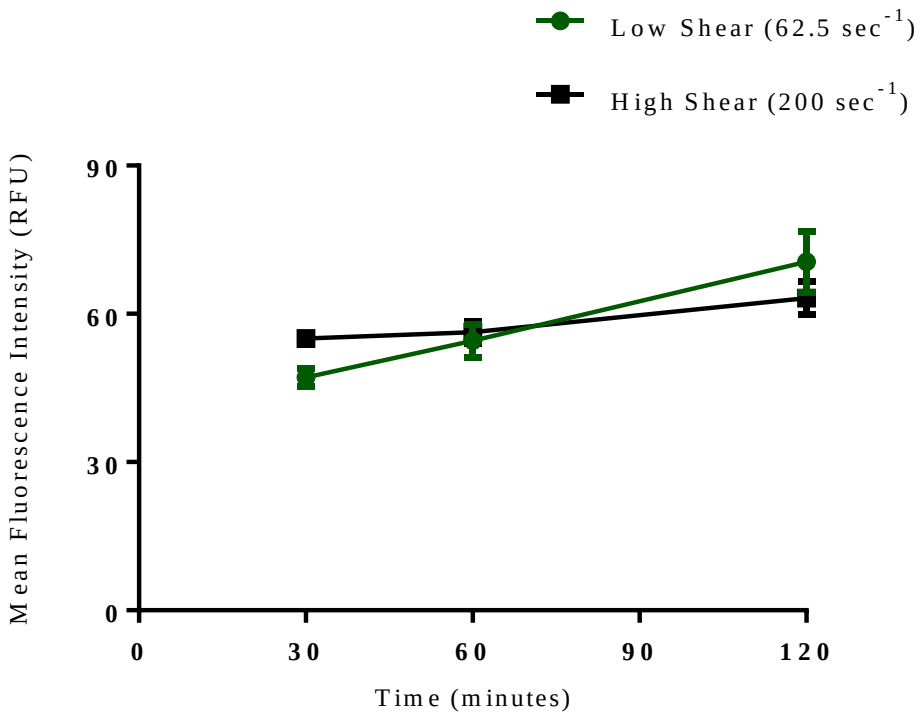

Figure 4- 3. Uptake of Anti-CD71 Bioconjugated CPSNPs after Low and High Shear Exposure. The mean fluorescence intensity of anti-CD71 particles was measured after 30, 60, and 120 minutes of shear exposure. No significant differences were seen between associations under differing shear conditions at any time point. Values are mean ± S.E.M. for $N \geq 6$.

Similarly to methoxy-PEG particles, Anti-CD71 particles showed no significant differences at any time points between associations of differing shear rates.

Results of Low Shear RhWT Particle-Cell Associations

A comparison of the results from experiments conducted on all three particle types (citrate, methoxy-PEG, and anti-CD71) under low shear conditions for 30, 60, and 120 minutes are shown in Figure 4-4. The average fluorescence intensity values for all three nanoparticle types were collected after low (62.5 sec^{-1}) shear rate exposure from the cone-plate viscometer.

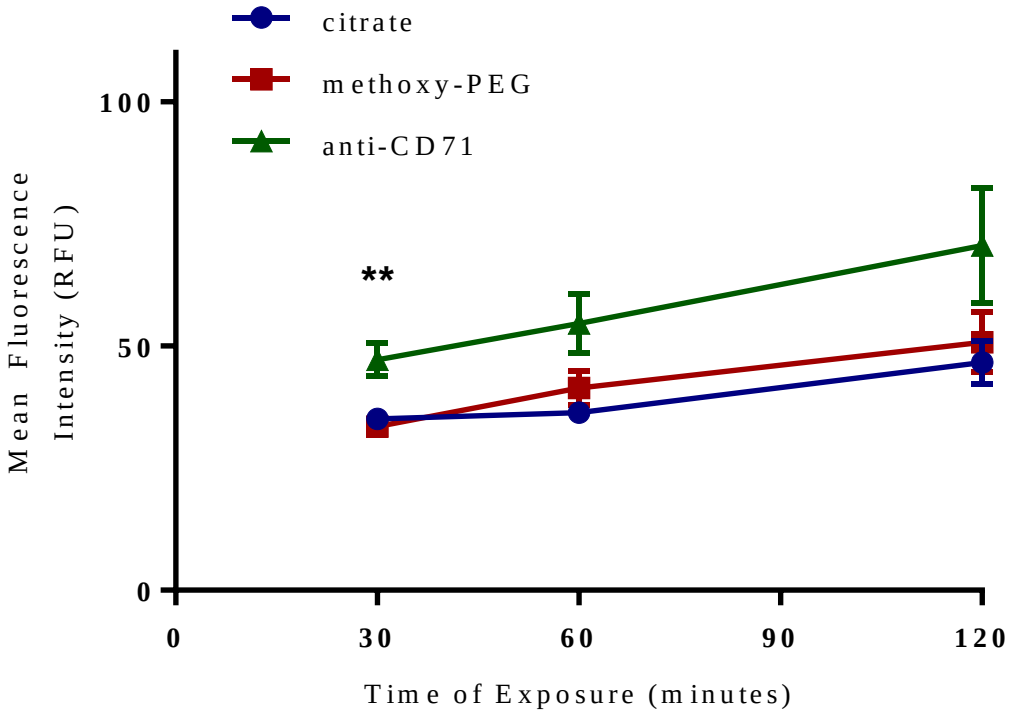

Figure 4-4. Uptake of CPSNPs after Low Shear Exposure. The mean fluorescence intensities of citrate, PEG, and anti-CD71 particles were measured after 30, 60, and 120 minutes of low shear exposure. Anti-CD71 particles showed significantly higher associations than citrate and methoxy-PEG particles after 30 minutes of exposure only ($p = 0.002$). **$P < 0.01$ for anti-CD71 particles compared with fluorescence of citrate and PEG particles. Values are mean ± S.E.M. for $N \geq 6$.

Anti-CD71 particles showed significantly higher associations than citrate and methoxy-PEG particles at 30 minutes ($p = 0.002$) and significantly higher associations than citrate at 60 minutes ($p = 0.022$). No significant differences between the uptake of varying particle types were seen at 120 minutes. Additionally, methoxy-PEGylated particles did not show significantly different uptake than citrate particles. Furthermore, both citrate and methoxy-PEG CPSNPs demonstrated significantly higher associations at 120 minutes as compared to 30 minutes indicating an increase in particle uptake by the cells over time ($p = 0.046, 0.037$). Anti-CD71 did not have significantly higher associations over time; however, trends indicate an increase in fluorescence intensity over time.

Results of High Shear RhWT Particle-Cell Associations

A comparison of the results from experiments conducted on all three particle types (citrate, methoxy-PEG, and anti-CD71) under high shear conditions for 30, 60, and 120 minutes are shown in Figure 4-5. The average fluorescence intensity values for all three nanoparticle types were collected after high (200 sec^{-1}) shear rate exposure from the cone-plate viscometer.

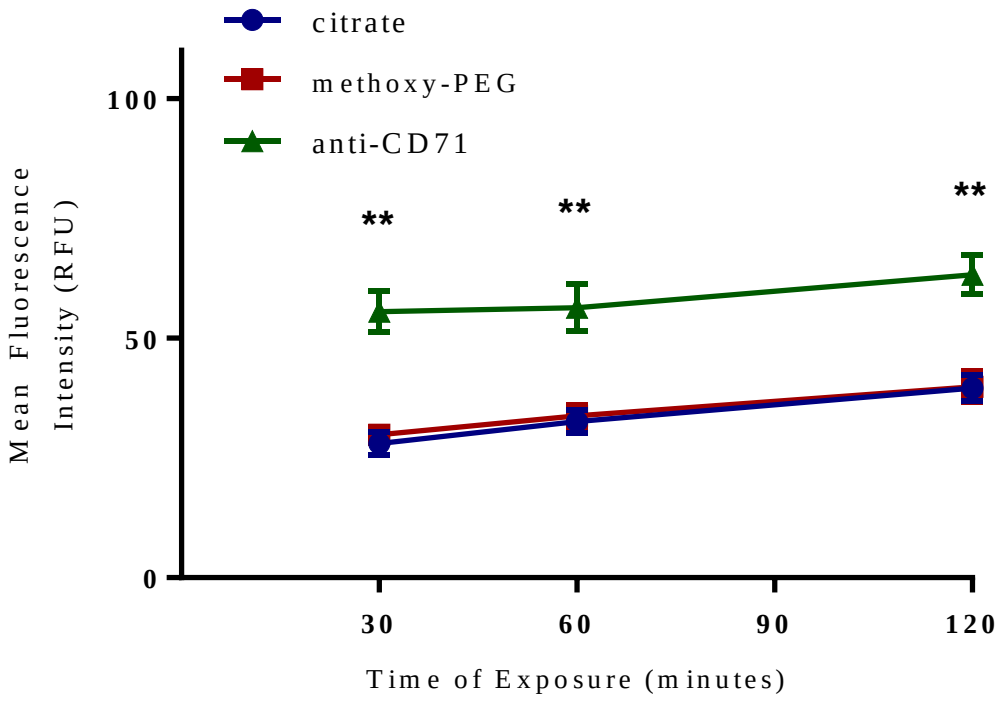

Figure 4- 5. Uptake of CPSNPs after High Shear Exposure. The mean fluorescence intensities of citrate, PEG, and anti-CD71 particles were measured after 30, 60, and 120 minutes of high shear exposure. Anti-CD71 particles showed significantly higher associations than citrate and methoxy-PEG particles for all three time points ($p = 0.001, 0.001, 0.001$). **$P < 0.01$ for anti-CD71 particles compared with fluorescence of citrate and PEG particles. Values are mean ± S.E.M. for $N \geq 6$.

Anti-CD71 particles showed significantly higher associations than citrate and methoxy-PEG particles at 30, 60, and 120 minutes ($p = 0.001, 0.001, 0.001$). Additionally, methoxy-PEGylated particles did not show significantly different uptake than citrate particles. Similarly to low shear conditions, associations at 120 minutes were significantly higher than at 30 minutes for citrate and methoxy-PEG CPSNPs, indicating an increase in particle uptake by the cells over time ($p = 0.010, 0.029$). However, anti-CD71 did not have significantly higher associations over time, indicating that maximum uptake was reached at earlier time points.

Figure 4-6 demonstrates the images at 10X magnification collected of the MDA-MB-231 breast cancer cells after exposure to either methoxy-PEG-functionalized or ant-CD71 bioconjugated Nile-red polystyrene microspheres for 30, 60, or 120 minutes under low shear (62.5 sec^{-1}) conditions.

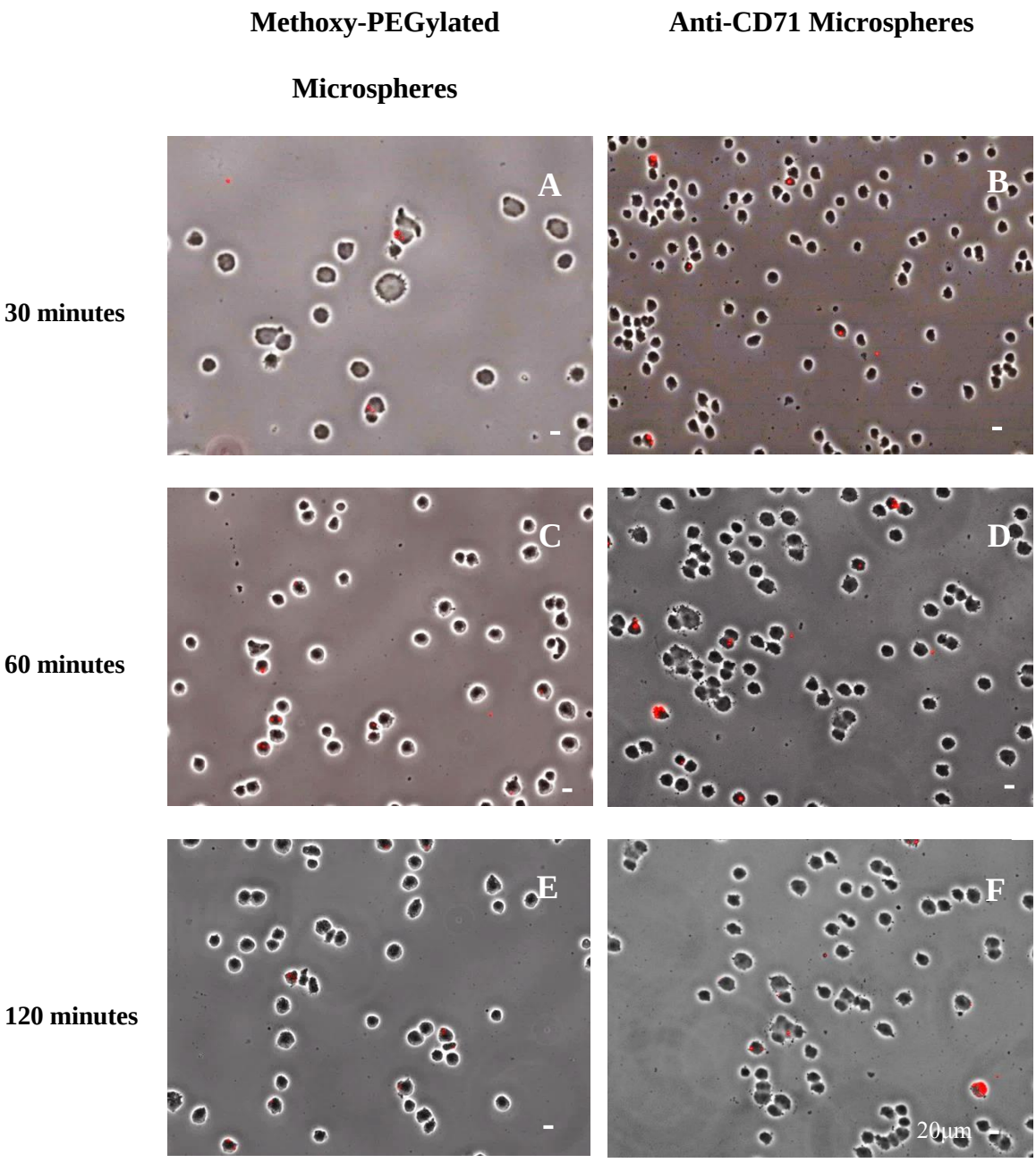

Figure 4- 6. Representative images of MDA-MB-231 Breast Cancer Cells Exposed to Nile-Red Methoxy-PEGylated microsphere vs. Cells exposed to Nile-Red Anti-CD71 Bioconjugated Microspheres Under Low Shear Conditions. A,B. Cells were exposed for 30 minutes. C,D. Cells were exposed for 60 minutes. E,F. Cells were exposed for 120 minutes.

The Nile-red microspheres with anti-CD71 surface bioconjugation appear to have greater accumulation than with methoxy-PEG functionalization on the surface of the MDA-MB-231 breast cancer cells. This appears to validate the results that the targeted bioconjugation technique provided enhanced associations under low shear conditions.

Chapter 5

Comparison of Polystyrene Microsphere and RhWT CPSNP Experiments

A normalized comparison between the results from experiments conducted on all three particle types (citrate, methoxy-PEG, and anti-CD71) and all three microsphere types (carboxy-terminated, methoxy-PEG, and anti-CD71) under low and high shear conditions for 30, 60, and 120 minutes are shown in Figures 5-1, 5-2, and 5-3, respectively.

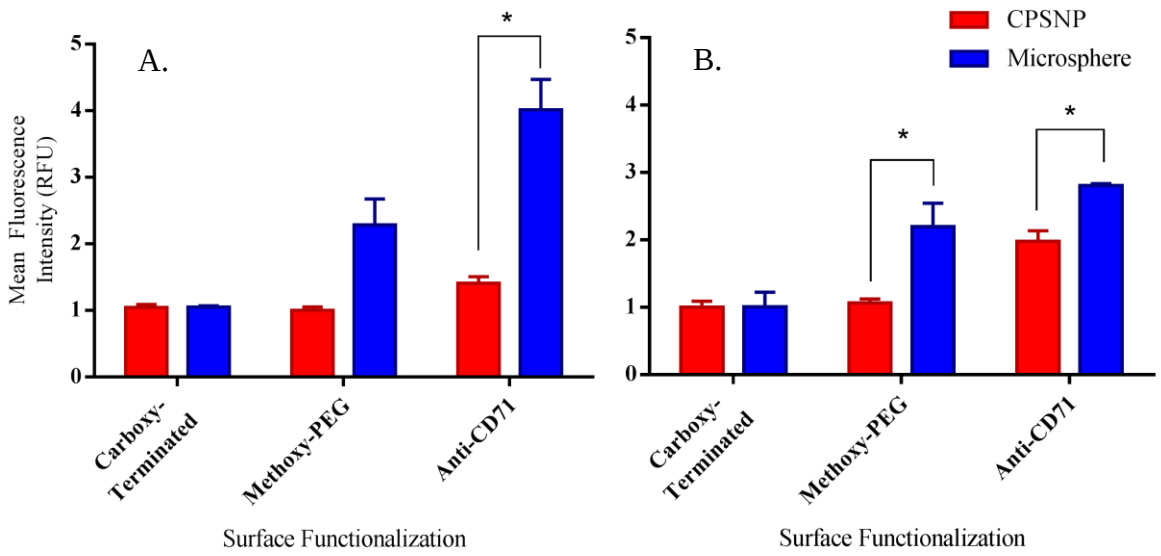

Figure 5-1. CPSNP- and Microsphere- Cell Uptake as a Function of Surface Functionalization after 30 minutes of Shear Exposure. A. Low Shear (62.5 sec -1) Exposure. B. High Shear (200 sec-1) Exposure. Anti-CD71 microspheres showed significantly higher associations than anti-CD71 particles for both low and high shear conditions ($p = 0.014, 0.026$). Methoxy-PEGylated microspheres showed significantly higher associations than methoxy-PEGylated particles under high shear conditions ($p – 0.029$). *$P < 0.05$ for microspheres compared with fluorescence of CPSNPs. Values are mean ± S.E.M. for $N \geq 4$.

After 30 minutes, Anti-CD71 bioconjugated microspheres showed significantly higher associations than anti-CD71 bioconjugated CPSNPs for both low and high shear conditions (p= 0.014, 0.026). Methoxy-PEGylated microspheres also showed significantly higher associations than corresponding CPSNPs under high shear conditions (p = 0.029). No significant differences were found between carboxy-terminated particles and microspheres for either high or low shear conditions.

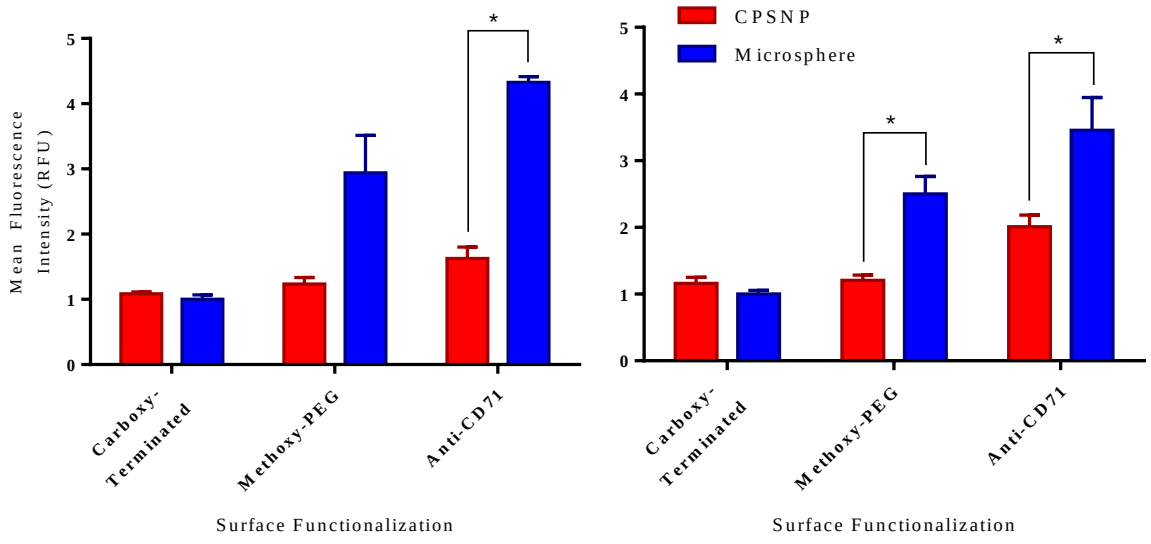

Figure 5-2. CPSNP- and Microsphere- Cell Uptake as a Function of Surface Functionalization after 60 minutes of Shear Exposure. A. Low Shear (62.5 sec -1) Exposure. B. High Shear (200 sec-1) Exposure. Anti-CD71 microspheres showed significantly higher associations than anti-CD71 particles for both low and high shear conditions (p = 0.001, 0.042). Methoxy-PEGylated microspheres showed significantly higher associations than methoxy-PEGylated particles under high shear conditions (p – 0.020). *P < 0.05 for microspheres compared with fluorescence of CPSNPs. Values are mean ± S.E.M. for N ≥ 4.

Likewise, after 60 minutes, Anti-CD71 bioconjugated microspheres showed significantly higher associations than anti-CD71 bioconjugated CPSNPs for both low and high shear

conditions (p= 0.001, 0.042). Methoxy-PEGylated microspheres also showed significantly higher associations than corresponding CPSNPs under high shear conditions (p = 0.020). No significant differences were found between carboxy-terminated particles and microspheres for either high or low shear conditions.

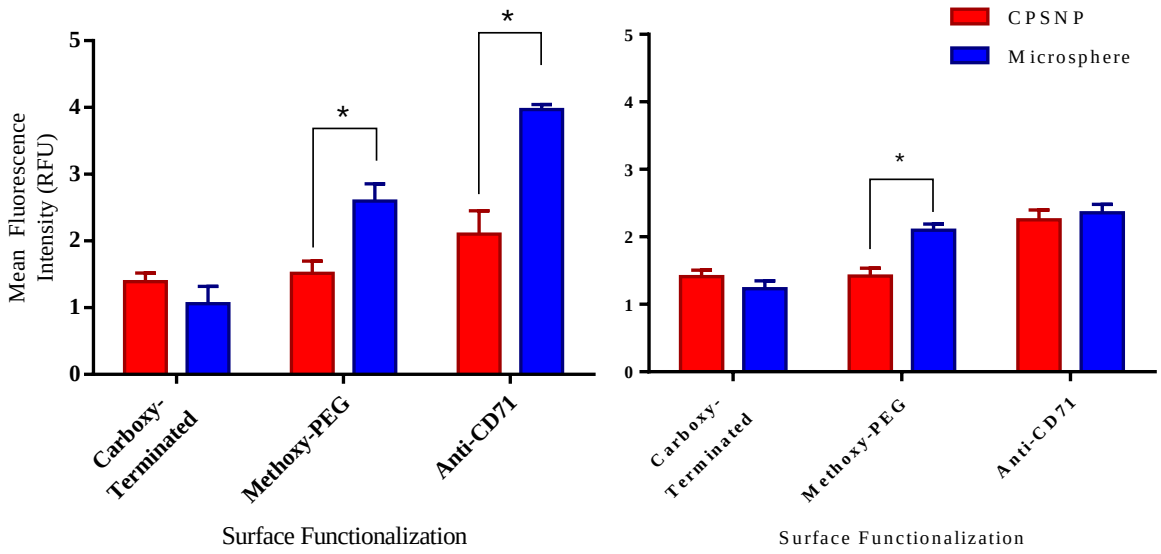

Figure 5-3. CPSNP- and Microsphere- Cell Uptake as a Function of Surface Functionalization after 120 minutes of Shear Exposure. A. Low Shear (62.5 sec -1) Exposure. B. High Shear (200 sec-1) Exposure. Anti-CD71 microspheres showed significantly higher associations than anti-CD71 particles for low and high shear conditions (p = 0.002). Methoxy-PEGylated microspheres showed significantly higher associations than methoxy-PEGylated particles under low and high shear conditions (p – 0.026, 0.001). *P < 0.05 for microspheres compared with fluorescence of CPSNPs. Values are mean ± S.E.M. for N ≥ 4.

After 120 minutes, Anti-CD71 bioconjugated microspheres showed significantly higher associations than anti-CD71 bioconjugated CPSNPs for low shear conditions only (p= 0.002). Methoxy-PEGylated microspheres also showed significantly higher associations than corresponding CPSNPs under both low and high shear conditions (p = 0.026, 0.001).

No significant differences were found between carboxy-terminated particles and microspheres for either high or low shear conditions.

Fluorescent Images of RhWT Particle- and Polystyrene Microsphere- Cell Associations

Results of viscometer experiments were validated using fluorescent images of the particle-cell associations following flow cytometry analysis. RhWT CPSNP-exposed breast cancer cell images were taken using only fluorescent microscopy, while Nile-Red Polystyrene microsphere-exposed breast cancer cell images were taken using both light and fluorescent microscopy to create an overlapping image. Figure 5-4 demonstrates the images at 20X magnification collected of the MDA-MB-231 breast cancer cells after exposure to either citrate-functionalized nanoparticles (left) or carboxy-terminated microspheres (right) for 30, 60, or 120 minutes under low shear (62.5 sec^{-1}) conditions.

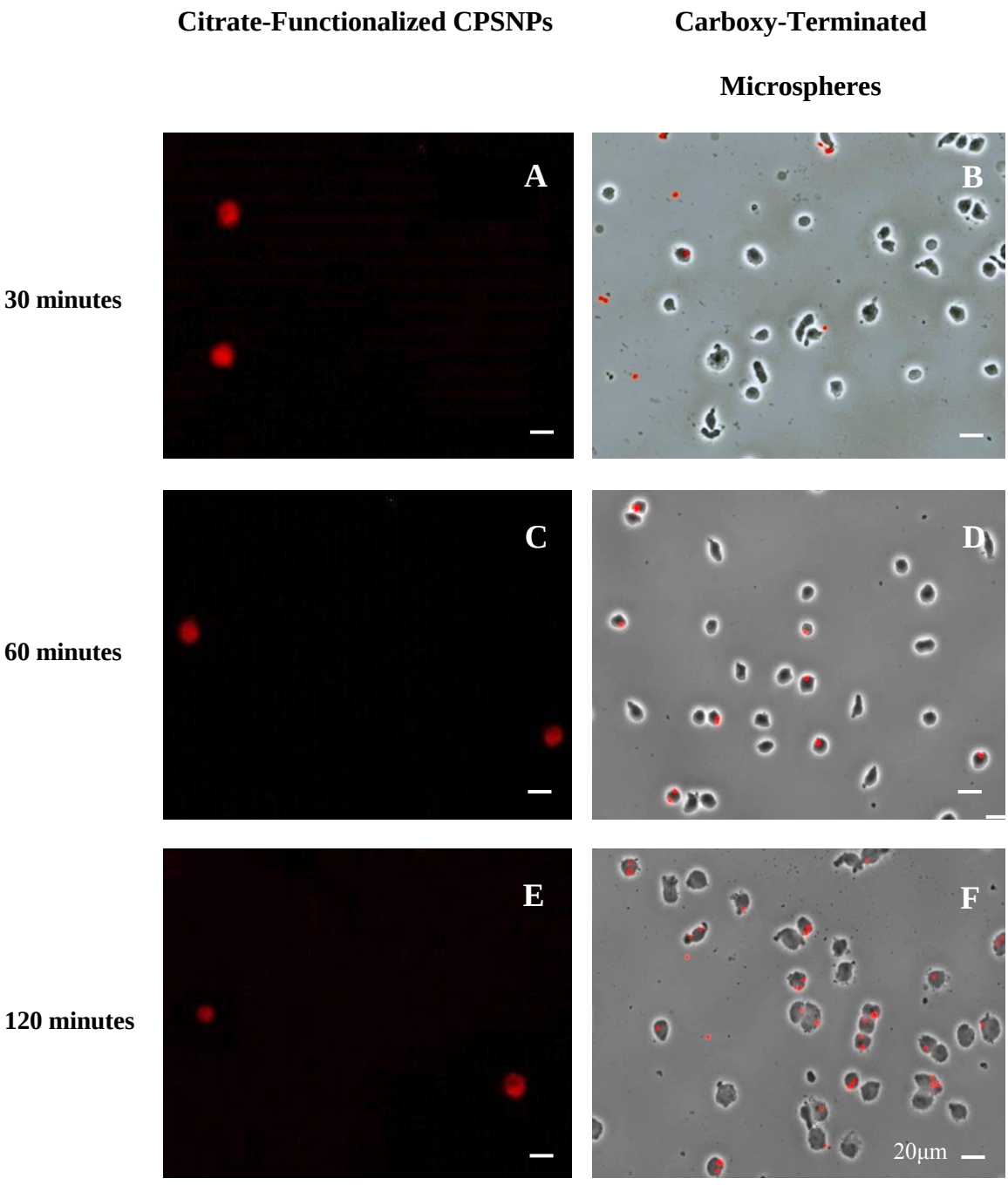

Figure 5- 4. Representative images of MDA-MB-231 Breast Cancer Cells Exposed to Rhodamine-WT from Citrate- CPSNPs vs. Cells exposed to Nile-Red Polystyrene Microspheres Under Low Shear Conditions. A,B. Cells were exposed for 30 minutes. C,D. Cells were exposed for 60 minutes. E,F. Cells were exposed for 60 minutes. E,F. Cells were exposed for 120 minutes.

The Nile-red polystyrene microspheres appear to accumulate on the surface of the MDA-MB-231 breast cancer cells, whereas the RhWT-CPSNPs appear to be dispersed throughout the cell. This indicates that the cells allowed to the nanoparticles to permeate through their membrane and undergo true uptake. In contrast, the microspheres appear to solely bind and accumulate on the surface of the cells without releasing the contents.

Chapter 6

Docetaxel Flow Migration Results

The following data show the immunohistochemistry, MTS assay, and preliminary flow migration results for testing the effects of doctaxel-encapsulated CPSNPs on the extravasation of metastatic breast cancer cells through the endothelium. Error bars on all graphs indicate standard error for n=6. * Above graphs indicates a p value of less than 0.05 and ** above graphs indicates a p-value of less than 0.01.

Results of Immunofluorescence Staining to Test for VCAM-1 Binding

To test for VCAM-1/VLA-4 binding, immunofluorescence staining was completed by probing MDA-MB-231 for VLA-4 and analyzing results via flow cytometry, as shown in Figure 6-1. Dot plots show the distribution of fluorescence intensities after staining with either Alexa Fluor 546 goat, anti-mouse secondary antibodies only (A), anti-CD49d (α_4) with secondary antibodies (B), or anti-CD29 (β_1) with secondary antibodies (C). The results were gated at 10, with fluorescence values greater than 10 indicating cells which were successfully tagged. The percentage on each graph represents the percentage of cells with greater fluorescence values than 10 and reflects the presence of receptors on the MDA-MB-231 cells.

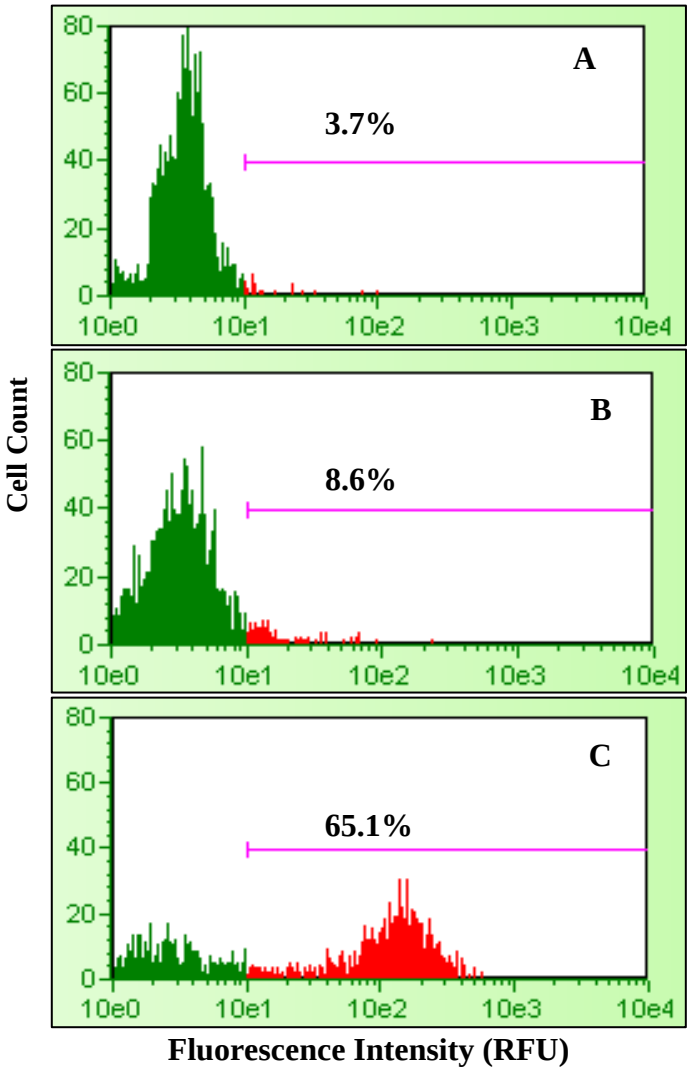

Figure 6-1. Flow Cytometry Analysis for Presence of VLA-4 Human MDA-MB-231 Metastatic Breast Cancer Cells. A. Background signal of Alexa Fluor 546 Goat, Anti-Mouse Secondary Antibody. B Signal of anti-CD49d (α_4) with secondary antibodies. [C] Signal of anti-CD29 (β_1) with secondary antibodies

The gated percentages of cells for each stain type were 3.7%, 8.6%, and 65.1% for secondary, α_4, and β_1 antibodies, respectively. The β_1 signal (C) was high, indicating the prevalence of the receptors on the surfaces of MDA-MB-231 cells. However, though α_4 levels were higher than the secondary signal alone, the levels were not high enough to

indicate significant prevalence of the receptors on the surfaces of the triple negative breast cancer cells.

Results of Docetaxel Dose Response Study

The results of the MTS Assay to test for the viability of MDA-MB-231 cells after exposure to different dosages of free docetaxel are shown in Figure 6-2. Normalized absorbance values were collected to reflect the viability of the breast cancer cells after docetaxel exposure with all data normalized to the vehicle. No treatment (NT) results are after exposure to DMEM only and vehicle results are after exposure to PBS with DMEM.

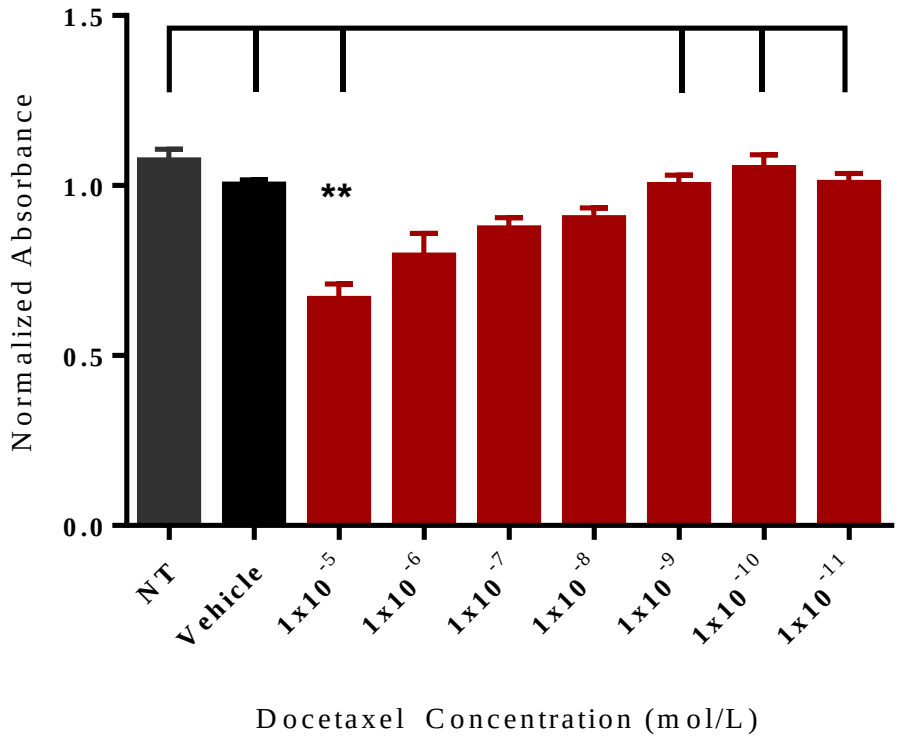

Figure 6-2. MDA-MB-231 Cell Viability Represented by Normalized Absorbance Values for Varying Free Docetaxel Concentrations. Free docetaxel was dissolved in

13% v/v ethanol in PBS. NT= No Treatment. Absorbance values of cells exposed to a $1x10^{-5}$ M concentration of docetaxel were significantly lower than absorbance of cells exposed to the vehicle, no treatment, and $1x10^{-9}$ M, $1x10^{-10}$ M, and $1x10^{-11}$M concentrations of docetaxel ($p = 0.001$). **$P < 0.01$ with respect to absorbance values of varying docetaxel concentrations. Values are mean ± S.E.M. for $N \geq 4$.

A free docetaxel concentration of $1x10^{-5}$ M significantly lowered the absorbance values of MDA-MB-231 breast cancer cells as compared to the vehicle, no treatment and $1x10^{-9}$ M, $1x10^{-10}$ M, and $1x10^{-11}$M concentrations of docetaxel ($p = 0.001$). Therefore, a concentration of $1x10^{-5}$ M of free docetaxel could be used for flow migration studies to test for the reduction in tumor cell extravasation by docetaxel drug exposure.

Free Docetaxel Flow Migration Results

Cell extravasation results after 4 hours of low (75 sec^{-1}) shear rate exposure are shown in Figure 6-3. The number of migrated cells reflects the amount of tumor cell extravasation through the endothelial monolayer after exposure to either the control (13% ethanol in PBS) or free docetaxel ($1x10^{-5}$ M or $1x10^{-6}$ M docetaxel in 13% ethanol in PBS). The migrated cells for each chamber were counted for five frames and averaged to determine the migrated cells/mm^2.

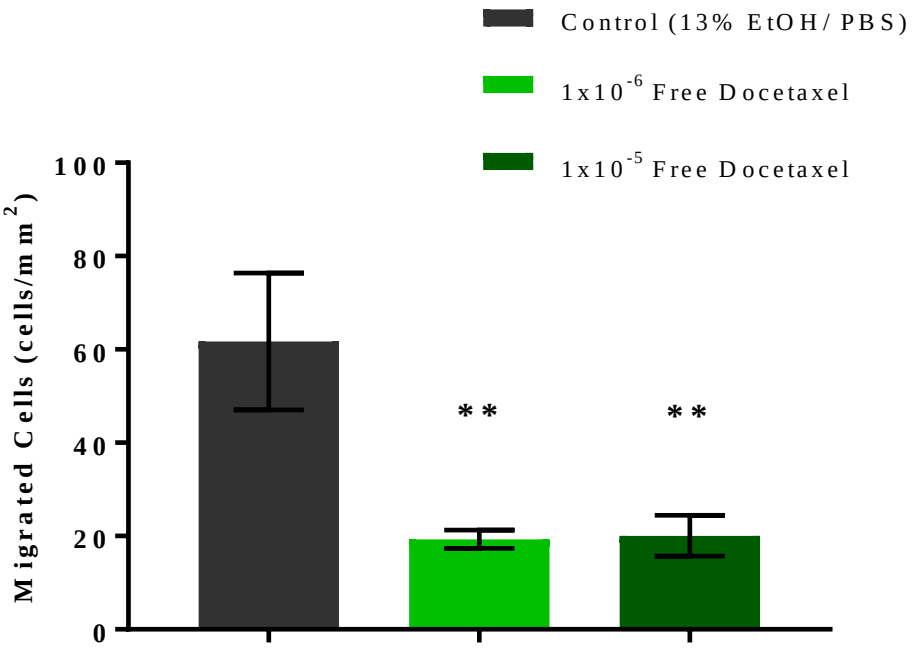

Figure 6-3. Cells Migrated Through Endothelial Monolayer After 4 Hours of Low Shear Exposure. Control is 13% v/v ethanol in PBS and free docetaxel is either $1x10^{-5}$M or $1x10^{-6}$ M docetaxel dissolved in 13% v/v ethanol in PBS. Free docetaxel concentrations of $1x10^{-5}$ M and $1x10^{-6}$ M significantly reduced cell migration as compared to the control ($p = 0.006, 0.007$). **$P < 0.01$ compared with control. Values are mean ± S.E.M. for $N \geq 6$.

Free docetaxel exposure significantly lowered the migration of cells through the endothelial monolayer as compared to the control for both $1x10^{-5}$ M and $1x10^{-6}$ M concentrations ($p = 0.006, 0.007$). Migration under low shear conditions was decreased by 68%, or an average of approximately forty-two cells/mm^2, for both $1x10^{-5}$ M and $1x10^{-6}$ M docetaxel concentrations.

Cell extravasation results after 4 hours of high (200 sec^{-1}) shear rate exposure are shown in Figure 6-4. The number of migrated cells reflects the amount tumor cell extravasation through the endothelial monolayer after exposure to either the control (13% ethanol in PBS) or free docetaxel ($1x10^{-5}$ M or $1x10^{-6}$ M docetaxel in 13% ethanol in

PBS). The migrated cells for each chamber were counted for five frames and averaged to determine the migrated cells/mm^2.

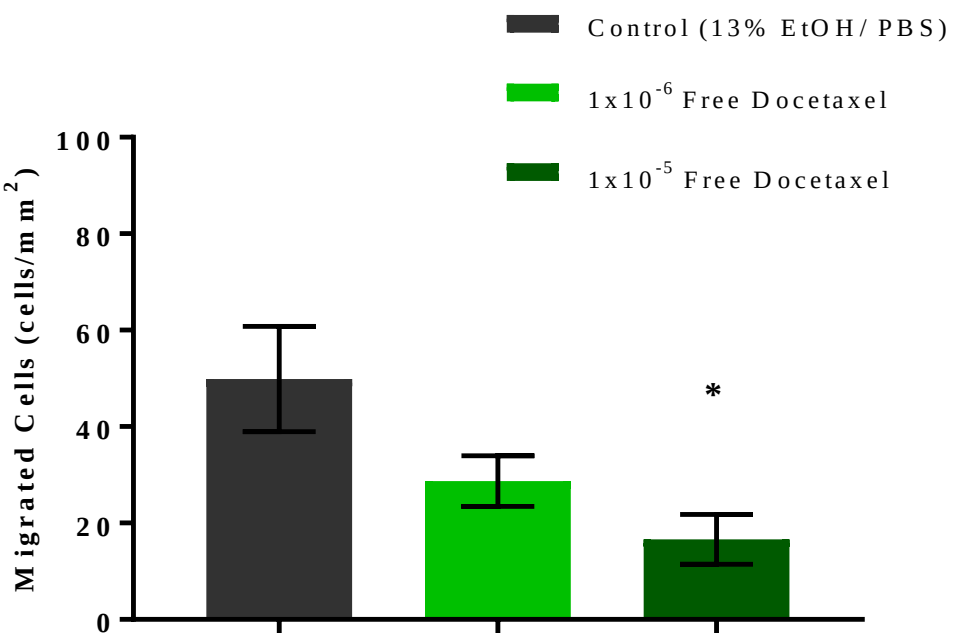

Figure 6-4. Cells Migrated Through Endothelial Monolayer After 4 Hours of High Shear Exposure. Control is 13% v/v ethanol in PBS and free docetaxel is either $1x10^{-5}$ M or $1x10^{-6}$ M docetaxel dissolved in 13% v/v ethanol in PBS. A free docetaxel concentration of $1x10^{-5}$ M significantly reduced cell migration as compared to the control ($p = 0.019$). *$P < 0.05$ compared with control. Values are mean ± S.E.M. for $N \geq 6$.

Migration under high shear conditions was significantly lowered after exposure to free docetaxel concentrations of $1x10^{-5}$ M only ($p= 0.019$) as compared to the control. Migration under high shear conditions with exposure to $1x10^{-5}$ M free docetaxel was decreased by 46%, or an average of twenty-one cells/mm^2. Though a docetaxel concentration of $1x10^{-6}$ M did decrease migration by 37%, no significant difference was seen as compared to the control.

Cell extravasation results after 4 hours of low (75 sec^{-1}) and high (200 sec^{-1}) shear rate exposure after exposure to either the control (13% ethanol in PBS) or free docetaxel ($1x10^{-5}$ M or $1x10^{-6}$ M docetaxel in 13% ethanol in PBS) are shown in Figure 6-5. The migrated cells for each chamber were counted for five frames and averaged to determine the migrated cells/mm^2.

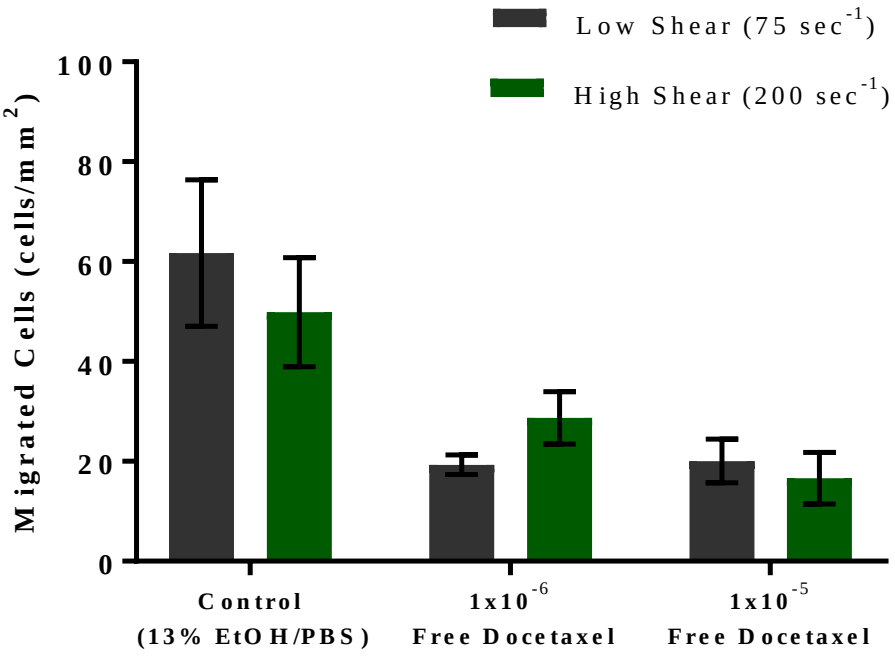

Figure 6-5. Cells Migrated Through Endothelial Monolayer After 4 Hours of Low or High Shear Exposure. Control is 13% v/v ethanol in PBS and free docetaxel is either $1x10^{-5}$ M or $1x10^{-6}$ M docetaxel dissolved in 13% v/v ethanol in PBS. No significant differences were seen for migrated cells under differing shear rates. Values are mean ± S.E.M. for $N \geq 6$.

For the control, $1x10^{-5}$ M and $1x10^{-6}$ M free docetaxel concentrations, differences between low and high shear rates were not significant.

Chapter 7

Discussion

Analysis of Nile-red Polystyrene Microsphere-Cell Associations

Microsphere experiments were completed to test the efficacy of the current bioconjugation approach and to provide a direct comparison to CPSNPs. After MDA-MB-231 breast cancer cells were exposed to carboxy-terminated, methoxy-PEGylated, and anti-CD71 bioconjugated microspheres in either low or high shear conditions, results showed that shear rate of flow had no significant effect on the cell-microsphere associations for carboxy-terminated and methoxy-PEGylated microspheres. However, under low shear conditions, anti-CD71 bioconjugated microspheres showed significantly greater associations with breast cancer cells at 30 and 120 minutes. It is likely that the hydrodynamic forces provided by the high shear rate of 200 sec^{-1} detached the microspheres from the surfaces of the breast cancer cells, leading to lower numbers of associations. Since the 1 μm-sized microspheres were too large to undergo endocytosis, they had relatively weak cell-surface binding and could more easily be detached. Furthermore, higher evaporation of fluid on the surface of the viscometer plate was seen for high shear rate experiments. It is possible that the increased fluid evaporation led to a higher concentration of microspheres and cells, thereby causing an increase in the number of cell and microsphere collisions. These collisions may also have led to an increase in microsphere detachment from the tumor cells.

Under low shear conditions, anti-CD71 microspheres showed significantly higher associations with breast cancer cells than methoxy-PEGylated and carboxy-

functionalized microspheres. Therefore, active targeting by the anti-CD71 microspheres was demonstrated to enhance cell associations. The antibody-receptor interactions can therefore be assumed to increase the strength of binding. Furthermore, methoxy-PEGylated microspheres showed significantly higher associations than carboxy-functionalized microspheres. Since the EPR effect is only applicable to a vessel wall in vivo, it does not play a role in increased associations seen by PEGylated microspheres. However, these results can be explained by the increased circulation time provided by the surface PEGylation of the microspheres.

Similarly to low shear conditions, high shear conditions demonstrated increased associations with PEGylation, as compared to carboxy-terminated microspheres, further proving the enhanced effect of increased circulation time. However, in contrast to low shear conditions, high shear conditions showed no increased associations by anti-CD71 microspheres, as compared to methoxy-PEGylated and carboxy-terminated microspheres at any time point. Therefore, active targeting of the breast cancer cells was not demonstrated under high shear conditions. As discussed earlier, this result can be explained by the decreased associations caused by the hydrodynamic forces from the shear flow. Nevertheless, trends should be confirmed by additional experiments to increase the sample size.

Furthermore, for both high and low shear conditions, no significant differences between time points for each microsphere functionalization type were seen. Therefore, max associations were reached by each microsphere functionalization type at an earlier time point than analyzed. This is most likely due to limited receptor-binding sites on the surface of the cells. If all the receptors sites were occupied, polystyrene microspheres

would have limited binding opportunities. However, anti-CD71 microspheres appear to decrease in associations between 60 and 120 minutes. Therefore, after time, the fluorescence intensity dropped from its maximum value to a lower value. This possibly indicates a decrease in the associations of anti-CD71 microspheres after long circulation times.

Analysis of RhWT-Encapsulated CPSNP-Cell Associations

Similarly to the polystyrene microspheres, differences in shear rate posed little to no effect on the uptake of CPSNPs by MDA-MB-231 breast cancer cells. With the exception of citrate particles at 30 minutes, there were no significant differences between shear rates, indicating that uptake of CPSNPs most likely was unaffected by the differences in shear conditions. However, unlike the polystyrene microsphere results, anti-CD71 bioconjugated microspheres were unaffected by the difference in shear rate. It is possible that the hydrodynamic forces from the shear fluid were not able to detach the particles from the tumor cells surfaces due to strong antibody-receptor binding. In addition, the particles may have been able to successfully undergo endocytosis, further protecting them from the effects of the high shear flow.

Under low shear conditions, anti-CD71 bioconjugated CPSNPs showed significantly higher uptake than methoxy-PEGylated and citrate-functionalized particles at 30 and 60 minutes and showed increased trends at 120 minutes. Active targeting of transferrin receptors was thereby demonstrated. Furthermore, methoxy-PEGylated CPSNPs did not show significantly higher uptake than citrate particles at any time.

Therefore, the increased circulation time provided by PEGylation demonstrated little to no positive effect on the particles under low shear.

Under high shear conditions, anti-CD71 CPSNPs showed significantly higher uptake at each time point than methoxy-PEG and citrate particles. Therefore, active targeting of the transferrin receptor was seen at all time points. Uptake of the anti-CD71 CPSNPs was therefore greater than the control particles. Similarly to the low shear results, since the methoxy-PEGylated particles did not show passive targeting in comparison to citrate particles, the increased circulation time posed no effect on particle uptake.

Time of exposure did have an effect on the uptake of both citrate and methoxy-PEGylated CPSNPs, with increased uptake over time, under both low and high shear conditions. Furthermore, though significant differences were not seen between time points under low shear conidionts, anti-CD71 CPSNPs showed an increasing trend in uptake over time. Therefore, maximum saturation levels of the particles by the cells may not have been reached within 120 minutes. Additional experiments should be completed to determine when the maximum saturation limit of the nanoparticles by the cells can be reached under low shear conditions. For high shear conditions these trends were not seen, indicating that the maximum saturation level was reached at earlier time points. Therefore, particle-receptor binding sites reached their maximum occupancy at or before 30 minutes of exposure.

Comparisons between RhWT CPSNPs and Nile-Red Polystyrene Microspheres

Normalized comparisons of RhWT-encapulated CPSNPs with Nile-red polystyrene microspheres show significantly higher associations for anti-CD71 microspheres at 30 and 60 minutes under both high and low shear conditions. Furthermore, methoxy-PEGylated microspheres showed significantly higher associations, as compared to methoxy-PEG CPSNPs at 30 and 60 minutes under low shear conditions and at 120 minutes under both high and low shear conditions. Therefore, the microspheres provided greater levels of passive and active targeting of the MDA-MB-231 human breast cancer cells than the particles. These results may be explained by the relatively large size of the microspheres. The greater size most likely increases the circulation time of the spheres, and also, allows for decreased degradation over time, as compared to nanoparticles. For methoxy-PEGylated and anti-CD71 bioconjugated CPSNPs in particular, high shear conditions created the greatest differences in the comparisons of associations, demonstrating heightened degradation and vulnerability to larger hydrodynamic forces. Since the nanoparticles are smaller and more susceptible to degradation, they may have had fewer opportunities for receptor binding as the microspheres, and therefore, reduced passive and active targeting.

Nevertheless, as validated through fluorescence microscopy images, the microspheres were not able to diffuse across the tumor cell membrane. Therefore, true uptake of the encapsulated contents was not achieved. The large size of the microspheres most likely prevents them from successfully permeating across the membrane. Therefore, though the microspheres did demonstrate more effective targeting, the CPSNPs

demonstrate greater delivery of encapsulated contents. Due to the small 20 nm size of the particles, the uptake of the nanoparticles would allow encapsulated chemotherapeutic drugs and imaging agents to be released within the tumor cells. However, in order to entirely prove that the nanoparticle contents have been released within the cell, confocal microscopy and other imaging tools would need to be utilized to image the inside of the cell.

Analysis of Immunostaining and MTS Assay Results

VLA-4 integrin expression on the surfaces of MDA-MB-231 breast cancer cells was evaluated to determine if VCAM-1on HPMEC cells was an appropriate binding target for flow migration studies. For the chemotaxis Boyden chamber to simulate extravasation, the tumor cells must first adhere to the endothelial cell surface before migration. After probing for both the α_4 and β_1 receptors on the surface of MDA-MB-231 breast cancer cells, β_1 expression was found to be significantly higher than the control. However, α_4 expression was found to only be slightly higher than the control. Therefore, though β_1 expression was high, low α_4 expression on MDA-MB-231 cells and presumed low VCAM-1 expression on unstimulated HPMEC indicate that VLA-4/VCAM-1 is a weak binding mechanism for the flow migration studies. However, since studies were undergone to compare results for different concentrations of docetaxel exposure and interactions between VLA-4 and VCAM-1 were not changed in any manner throughout the experiments., a weak adherence to the endothelial monolayer would have little impact on the results.

An MTS proliferation assay was also used to validate the use of a chemotaxis Boyden chamber to study the effects of docetaxel on tumor cell extravasation. A dose response study demonstrated that after exposure to a free docetaxel concentration of $1x10^{-5}$ M in 13% ethanol in PBS, cell viability was significantly reduced, as compared to the control. Specifically, cell viability was reduced by approximately 33%, as compared to media alone. Furthermore, the cell viability for a $1x10^{-5}$M concentration of free docetaxel was significantly lower than $1x10^{-9}$ M, $1x10^{-10}$ M, and $1x10^{-11}$M concentrations. Therefore, a free docetaxel concentration of $1x10^{-5}$M in 13% ethanol/PBS could be used for flow migration studies to successfully decrease breast cancer cell viability, thereby reducing cell extravasation.

Analysis of Docetaxel Flow Migration Studies

The effects of free docetaxel on the extravasation of MDA-MB-231 breast cancer cells through a cell monolayer of HPMEC were tested using a modified chemotaxis Boyden chamber flow migration device. Though a drug concentration of $1x10^{-6}$ M did not show significantly lower absorbance values than the vehicle and no treatment for the MTS assay, the lower concentration was tested, in addition to $1x10^{-5}$ M, to more accurately represent concentrations of encapsulated docetaxel in CPSNPs. After 4 hours of low and high shear flow, the number of cells migrated through the endothelial monolayer was significantly lowered after exposure to a $1x10^{-5}$ concentration of free docetaxel in 13% ethanol/DPBS, as compared to 13% ethanol/DPBS alone. However, for a $1x10^{-6}$ M concentration of docetaxel, a significant decrease in migrated cells was only

seen under low shear conditions, though high shear conditions did indicate a trend for lowered extravasation. Therefore, under low shear conditions, both docetaxel concentrations were able to successfully hinder tumor cell extravasation, while under high shear conditions, only an increased drug concentration of $1x10^{-5}$ M was able to mitigate extravasation. Lastly, no differences were found in cell migration with differing shear rates.

These results provide two important conclusions for future studies testing the effects of docetaxel-encapsulated CPSNPs on cell extravasation. Firstly, since the relatively low concentrations of $1x10^{-5}$ M and $1x10^{-6}$ M were sufficient in hindering cell migration though the endothelial monolayer for almost all shear conditions, docetaxel-encapsulated CPSNPs would most likely also be able to lower cell extravasation. Though a $1x10^{-6}$ M of free docetaxel was only able to lower migration under low shear conditions, migration under high shear conditions did show a decreased trend. This indicates the potential for a lower encapsulated drug concentration within the CPSNPs to prove effective in reducing cell metastasis. Secondly, the lack of significant differences in cell migration between shear flow conditions indicates that differences in shear flow in circulation have minimal effect on the efficacy of docetaxel on hindering cell extravasation. Therefore, further flow migration studies should be conducted to test the efficacy of docetaxel-encapsulated CPSNPs as chemotherapeutic delivery vehicle to prevent tumor cell metastasis.

Chapter 8

Conclusions

Summary of Findings

In this study, the efficacy of the bioconjugation technique for calcium phosphosilicate nanoparticles to actively target human metastatic breast cancer was successfully demonstrated. Under both low and high shear flow conditions *in vitro*, the nanoparticles were able to actively target receptors on the surfaces of MDA-MB-231 human breast cancer cells. In addition, shear flow rates in circulation were shown to minimally effect the targeting of the nanoparticles, thereby providing evidence that active targeting is possible even in areas of circulation with high exposure to hydrodynamic forces. Furthermore, the active targeting technique was further validated by bioconjugated fluorescent, polystyrene microspheres. A comparison between both CPSNPs and polystyrene microspheres demonstrated the advantages of the 20 nm particles in regards to particle uptake and encapsulated drug release. Since high shear conditions only decreased associations for anti-CD71 microspheres and not for CPSNPs, it was shown that active receptor targeting and uptake was stronger for the nanoparticles. CPSNPs were therefore demonstrated to be a strong delivery vehicle in targeting and delivering encapsulated chemotherapeutics in both high and low shear circulation.

Additionally, the effects of docetaxel in hindering cell extravasation were demonstrated in this study and the chemotaxis Boyden chamber was validated as a useful tool in simulating cell migration across the endothelium under flow conditions. Substantial differences in the wall shear stress had no significant effect on the migration

of cells through the monolayer, thereby indicating the possibility that docetaxel-CPSNPs would be able to hinder cell extravasation and subsequent metastasis, even in areas of high shear circulation. In summary, the evidence that docetaxel is able to mitigate cell migration provides an indication that docetaxel-encapsulated CPSNPs have a strong potential to serve as a drug delivery vehicle in preventing tumor cell metastasis.

Future Directions

To verify that the CPSNPs have successfully ben engulfed by the cells and that the encapsulated fluorophore within the core of the CPSNPs has been released, imaging analysis techniques or microscopy must be carried out. Since flow cytometry measures the fluorescence outside of the cells, as well, it is possible that the particles have only bound to the surface of the cells. If the particles are not engulfed by the cell, the encapsulated drug will not be able to reach the cell, since the nanoparticles will not dissolve. Hence, confocal microscopy for example, can be used to image sectional planes of a fluorescent cell and reconstruct a three-dimensional image. This will prove to be a useful tool in analyzing the internal uptake of the nanoparticles.

In addition, since maximum saturation levels were seen at early time points for the particles under certain flow conditions, time points below 30 minutes should be studied. By studying earlier time points, the minimum time for the nanoparticles to reach the maximum saturation can be determined. Since the shorter the time it takes for the particles to target the cells and releases its contents the better, it is useful to know how efficient the particles are in reaching the tumor cells.

Due to limitations in the ability to measure the concentration of docetaxel encapsulated in docetaxel CPSNPs, flow migration studies were not carried out using the particles. However, once the drug concentration can be determined, flow migration studies using the modified chemotaxis Boyden chamber can provide insight into the effects of the particles in hindering cell metastasis. Furthermore, by testing citrate, methoxy-PEG, and anti-CD71 CPSNPs, the ability of the nanoparticles to actively target cells to mitigate cell migration can be determined. This will provide insight into the ability of the particles to successfully reach and target tumor cells before they bind and migrate through the endothelium.

Lastly, since the overall purpose of this study was to develop and analyze the efficacy of a tumor-targeted, chemotherapeutic drug delivery vehicle, *in vivo* experiments should be conducted using murine animal models. By demonstrating that these novel nanoparticles can indeed target and delivery chemotherapeutic drugs to tumor cells in circulation, calcium phosphosilicate nanoparticles can be moved one step closer to clinical trial for the treatment and detection of breast cancer.

Bibliography

1. National Cancer Institute. Breast Cancer Treatment. *Www.Cancer.Gov* 1–32 (2013).
2. Siegel, R., Ma, J., Zou, Z. & Jemal, A. Cancer statistics, 2014. *CA. Cancer J. Clin.* **64,** 9–29 (2014).
3. Gout, S. & Huot, J. Role of cancer microenvironment in metastasis: focus on colon cancer. *Cancer Microenviron.* **1,** 69–83 (2008).
4. Reed, A. E. M., Kutasovic, J. R., Lakhani, S. R. & Simpson, P. T. Invasive lobular carcinoma of the breast: morphology, biomarkers and 'omics. *Breast Cancer Res.* **17,** 12 (2015).
5. Valastyan, S. & Weinberg, R. A. Tumor metastasis: Molecular insights and evolving paradigms. *Cell* **147,** 275–292 (2011).
6. Suresh, S. Biomechanics and biophysics of cancer cells. *Acta Mater.* **55,** 3989–4014 (2007).
7. Suva, L. J., Griffin, R. J. & Makhoul, I. Mechanisms of bone metastases of breast cancer. *Endocr. Relat. Cancer* **16,** 703 (2009).
8. Kelly, T. *et al.* Expression of heparanase by primary breast tumors promotes bone resorption in the absence of detectable bone metastases. *Cancer Res.* **65,** 5778–5784 (2005).
9. Kufe, D. W. *et al.* Pathophysiology of the Metastatic Process. 2–4 (2003).
10. Liu, B. M. and Y. Microvascular Transport and Tumor Cell Adhesion in the Microcirculation. *Ann. Biomed. Eng.* **40,** 2442–2455 (2012).

11. Kumar, S. & Weaver, V. M. Mechanics, malignancy, and metastasis: The force journey of a tumor cell. *Cancer Metastasis Rev.* **28,** 113–127 (2009).

12. Garcia-Briones, M. A. & Chalmers, J. J. Flow parameters associated with hydrodynamic cell injury. *Biotechnol. Bioeng.* **44,** 1089–98 (1994).

13. Margaret J. Slattery, Shile Liang, and C. D. Distinct role of hydrodynamic shear in leukocyte-facilitated tumor cell extravasation. *Am. J. Physiol. - Cell Physiol.* **288,** C831-9 (2005).

14. Thamilselvan, V., Craig, D. H. & Basson, M. D. FAK association with multiple signal proteins mediates pressure-induced colon cancer cell adhesion via a Src-dependent PI3K/Akt pathway. *FASEB J. Res. Commun.* **21,** 1730–1741 (2007).

15. Ley, K. & Huo, Y. VCAM-1 is critical in atherosclerosis. *J. Clin. Invest.* **107,** 1209–1210 (2001).

16. Liang, S. & Dong, C. Integrin VLA-4 enhances sialyl-Lewisx/a-negative melanoma adhesion to and extravasation through the endothelium under low flow conditions. *Am J Physiol. Cell Physiol.* **295,** C701–C707 (2008).

17. Iademarco, M. F., Barks, J. L. & Dean, D. C. Regulation of vascular cell adhesion molecule-1 expression by IL-4 and TNF-alpha in cultured endothelial cells. *J. Clin. Invest.* **95,** 264–271 (1995).

18. Adair, J. H. Calcium phosphate nanocomposite particles: a safer and more effective alternative to conventional chemotherapy? *Futur. Oncol.* **5,** 279–281 (2009).

19. Carelle, N. *et al.* Changing patient perceptions of the side effects of cancer chemotherapy. *Cancer* **95,** 155–63 (2002).

20. Baker, J. *et al.* Docetaxel-related side effects and their management. *Eur. J. Oncol. Nurs.* **13,** 49–59 (2009).

21. Rowinsky, E. K. The development and clinical utility of the taxane class of antimicrotubule chemotherapy agents. *Annu. Rev. Med.* **48,** 353–74 (1997).

22. Barth, B. M. *et al.* PhotoImmunoNanoTherapy Reveals an Anticancer Role for Sphingosine Kinase 2 and Dihydrosphingosine-1-Phosphate. *ACS Nano* **7,** 2132–2144 (2013).

23. Morgan, T. T. *et al.* Encapsulation of Organic Molecules in Calcium Phosphate Nanocomposite Particles for Intracellular Imaging and Drug Delivery. *Nano Lett.* **8,** 4108–4115 (2008).

24. Sharma, R. *et al.* Bioconjugation of Calcium Phosphate Nanoparticles for Selective Targeting of Human Breast and Pancreatic Cancers In Vivo. *ACS Nano* **4,** 1279–1287 (2010).

25. Russin, T. J. *et al.* Near-Infrared Emitting Fluorophore- for In Vivo Imaging of Human Breast. *ACS Nano* **2,** 2075–2084 (2008).

26. Tacelosky, D. M. *et al.* Calcium phosphosilicate nanoparticles for imaging and photodynamic therapy of cancer. *Discov Med* **13,** 275–285 (2012).

27. Greish, K. Enhanced Permeability and Retention (EPR) Effect for Anticancer Nanomedicine Drug Targeting. *Cancer Nanotechnol. Methods Mol. Biol.* **624,** 25–37 (2010).

28. Bamrungsap S, Zhao Z, Chen T, Wang L, Li C, Fu T, T. W. Nanotechnology in therapeutics: a focus on nanoparticles as a drug delivery system. *Bulletin of the Astronomical Institutes of Czecheslovakia* **29,** (1978).

29. Hughes, K. Encapsulation of Docetaxel in Calcium Phosphosilicate Nanoparticles and the Effects of Bioconjugation. **1,** (The Pennsylvania State University, 2013).

30. Coors, E. a, Seybold, H., Merk, H. F. & Mahler, V. Polysorbate 80 in medical products and nonimmunologic anaphylactoid reactions. *Ann. Allergy. Asthma Immunol.* **95,** 593–9 (2005).

31. Tabakovic, A. Investigation of Laundering and Dispersion Approaches for Silica and Calcium Phosphosilicate Composite Nanoparticles Synthesized in Reverse Micelles. *PhD Proposal* **1,** (The Pennsylvania State University, 2015).

32. Tang, X. Dye-Doped Calcium Phosphosilicate Nanoparticles for Early Detection of Human Cancers (Doctoral dissertation). (The Pennsylvania State University, 2016).

33. Zhang, P., Ozdemir, T., Chung, C.-Y., Robertson, G. P. & Dong, C. Sequential binding of αVβ3 and ICAM-1 determines fibrin-mediated melanoma capture and stable adhesion to CD11b/CD18 on neutrophils. *J. Immunol.* **186,** 242–254 (2011).

34. Shile, L. Hydrodynamic Effects on Intercellular Interactions of Tumor Cells with Leukocytes and Endothelium (Doctoral Dissertations. (The Pennsylvania State University 2008).

35. Neelamegham, S. *et al.* Modeling the reversible kinetics of neutrophil aggregation under hydrodynamic shear. *Biophys. J.* **72,** 1527–1540 (1997).

36. Taylor, a D., Neelamegham, S., Hellums, J. D., Smith, C. W. & Simon, S. I. Molecular dynamics of the transition from L-selectin- to beta 2-integrin-dependent neutrophil adhesion under defined hydrodynamic shear. *Biophys. J.* **71,** 3488–500 (1996).

37. Harter, L. The Effect of Bioconjugation of Calcium Phosphosilicate Nanoparticles on Breast Cencer Cell Associations Under Shear Conditions (Dissertation). (The Pennsylvania State University 2012).

38. Weidert, E., Pohler, S. E., Gomez, E. W. & Dong, C. Actinomyosin Contraction , Phosphorylation of VE- Cadherin , and Actin Remodeling Enable Melanoma-Induced Endothelial Cell-Cell Junction Disassembly. *PLoS One* **9,** (2014).

39. Dong, Cheng; Slattery, Margaret; Rank, Bradley; You, J. In Vitro Characterization and Micromechanics of Tumor Cell Chemotactic Protrusion, Locomotion, and Extravasation. *Ann. Biomed. Eng.* **30,** 344–355 (2002).

40. Slattery, M. J. & Dong, C. Neutrophils influence melanoma adhesion and migration under flow conditions. *Int. J. Cancer* **106,** 713–722 (2003).

41. Dong, C., Slattery, M. & Liang, S. Micromechanics of tumor cell adhesion and migration under dynamic flow conditions. *Front. Biosci.* **10,** 379–384 (2005).

Appendix A

Nile-Red Polystyrene Microsphere Flow Cytometry Data

All values reflect mean fluorescence intensity in relative fluorescence intensity units (RFU) collected from flow cytometer readings. Values are mean ± S.E.M. for $N \geq 4$.

Low Shear (62.5 sec^{-1}) Conditions

Table A-1. Carboxy-Terminated Microsphere Flow Cytometry Results

30 minutes	139	132	132	141	126	132	Mean 134± 5
60 minutes	99	98	132	133	151	149	127± 20
120 minutes	118	111	112	141	161	166	135± 20

Table A-2. Methoxy-PEGylated Microsphere Flow Cytometry Results

30 minutes	390	387	201	179	-	-	Mean 289± 100
60 minutes	382	608	250	251	-	-	373± 200
120 minutes	427	349	292	251	-	-	330± 70

Table A-3. Anti-CD71 Bioconjugated Microsphere Flow Cytometry Results

30 minutes	367	679	450	540	-	-	Mean 509± 100
60 minutes	492	567	630	507	-	-	540± 60
120 minutes	550	448	403	480	653	486	503± 80

High Shear (200 sec^{-1}) Conditions

Table A-4. Carboxy-Terminated Microsphere Flow Cytometry Results

30 minutes	119	114	133	135	133	128	Mean 127± 8
60 minutes	102	104	127	140	150	134	126± 20
120 minutes	104	108	184	190	172	174	156± 40

Table A-5. Methoxy-PEGylated Microsphere Flow Cytometry Results

30 minutes	376	330	430	158	179	192	Mean 278± 100
60 minutes	268	311	426	258	-	-	316± 70
120 minutes	239	228	248	277	288	308	265± 30

Table A-6. Anti-CD71 Bioconjugated Microsphere Flow Cytometry Results

30 minutes	335	295	302	461	380	-	Mean 354± 70
60 minutes	440	702	508	437	307	224	436± 200
120 minutes	265	311	233	321	305	350	297± 40

Appendix B

Rhodamine-WT CPSNP Flow Cytometry Data

All values reflect mean fluorescence intensity in relative fluorescence intensity units (RFU) collected from flow cytometer readings. Values are mean ± S.E.M. for N ≥ 6.

Low Shear (62.5 sec^{-1}) Conditions

Table B-1. Citrate-Functionalized CPSNP Flow Cytometry Results

30 minutes	31.0	32.4	32.4	39.2	39.1	36.0	Mean 35.0± 4
60 minutes	38.2	37.3	37.2	32.1	34.9	38.4	36.4± 2
120 minutes	42.4	50.8	39.0	52.7	62.3	32.3	46.6± 10

Table B-2. Methoxy-PEGylated CPSNP Flow Cytometry Results

30 minutes	35.4	37.6	31.7	38.2	26.4	32.0	Mean 33.5±4
60 minutes	31.7	36.0	34.9	45.1	51.6	49.1	41.4± 8
120 minutes	47.1	38.6	72.5	66.9	40.4	39.1	50.8± 20

Table B-3. Anti-CD71 Bioconjugated CPSNP Flow Cytometry Results

30 minutes	50.6	49.2	57.1	48.2	46.1	31.6	Mean 47.1± 9
60 minutes	44.5	46.3	76.2	69.6	49.5	41.3	54.6± 10
120 minutes	45.8	48.9	93.7	117.6	62.9	54.3	70.5± 30

High Shear (200 sec^{-1}) Conditions

Table B-4. Citrate-Functionalized CPSNP Flow Cytometry Results

30 minutes	27.5	22.0	32.7	37.1	27.7	21.2	Mean 28.0± 6
60 minutes	34.4	33.6	37.2	39.1	28.6	22.6	32.6± 6
120 minutes	41.4	49.4	44.3	34.1	33.5	34.8	39.6± 7

Table B-5. Methoxy-PEGylated CPSNP Flow Cytometry Results

30 minutes	37.3	26.3	28.5	28.1	31.4	27.7	Mean 29.9± 4
60 minutes	36.8	37.2	31.0	26.9	29.4	41.5	33.8± 6
120 minutes	38.1	37.9	42.1	34.6	54.5	31.6	39.8± 8

Table B-6. Anti-CD71 Bioconjugated CPSNP Flow Cytometry Results

30 minutes	63.3	63.1	35.8	50.9	62.0	57.7	Mean 55.5± 10
60 minutes	59.5	53.1	47.8	44.2	78.4	54.9	56.3± 10
120 minutes	73.8	59.5	51.2	57.6	76.4	60.6	63.2± 10

Appendix C

Flow Migration Data

Absorbance Values for MTS Assay

All values reflect absorbance values and were measured at 490 nm using a 96-well plate reader. Values are mean ± S.E.M. for $N \geq 6$.

Table C-1. MTS Assay Results. Values indicate absorbance by MDA-MB-231 cells after treatment with free docetaxel. NT = No Treatment.

NT	Vehicle	$1x10^{-5}$ M	$1x10^{-6}$ M	$1x10^{-7}$ M	$1x10^{-8}$ M	$1x10^{-9}$ M	$1x10^{-10}$ M	$1x10^{-11}$ M
0.62	0.53	0.37	0.52	0.47	0.54	0.56	0.48	0.51
0.67	0.63	0.36	0.45	0.43	0.45	0.62	0.71	0.63
0.50	0.65	0.22	0.19	0.54	0.55	0.51	0.73	0.66
0.75	0.60	0.45	0.44	0.53	0.54	0.55	0.67	0.58
0.71	0.58	0.56	0.66	0.50	0.69	0.72	0.66	0.71
0.63	0.62	0.44	0.60	0.67	0.50	0.66	0.54	0.55
Mean	1.00± 0.04	0.66± 0.10	0.79± 0.20	0.87± 0.08	0.90± 0.08	1.0± 0.08	1.1± 0.10	1.0± 0.07
0.71± 0.09								

Flow Migration Under Low and High Shear

All values reflect number of migrated cells per square mm and were counted using a NIKON TE-2000 microscope. Values are mean ± S.E.M. for N ≥ 6.

Table C-2. Flow Migration Results. Low shear rate is 75 sec^{-1} and values indicate mean migrated cells (per mm^2) for each chamber.

Exposure to Control		$1x10^{-6}$ M Docetaxel Exposure	$1x10^{-5}$ M Docetaxel Exposure
34		22	16
109		18	23
53		17	31
33		11	10
78		6	9
-		15	6
Mean	62 ± 10	19 ± 2	20 ± 4

Table C-3. Flow Migration Results. High shear rate is 200 sec^{-1} and values indicate mean migrated cells (per mm^2) for each chamber.

Exposure to Control		$1x10^{-6}$ M Docetaxel Exposure	$1x10^{-5}$ M Docetaxel Exposure
58		29	36
30		44	13
91		13	34
26		23	4
36		13	8
58		20	4
Mean	50 ± 10	29 ± 5	17 ± 10

VIRGINIA GONZALEZ

VLG5065@PSU.EDU

EDUCATION

The Pennsylvania State University
Schreyer Honors College Scholar in Integrated Undergraduate/Graduate Program
Master of Science, Bioengineering
Bachelor of Science, Biomedical Engineering, Biomaterials Concentration

WORK EXPERIENCE

Pharmaceutical Development and Manufacturing Sciences – Johnson & Johnson Malvern, PA
Co-Op/Analyst *May 2016 - Present*

- Support the cell banking team within the API-Large Molecule Department in the production and testing of Development Cell Banks in both GMP and GLP laboratories for Janssen Pharmaceutical Companies
- Lead the experimentation of ten cell lines for material qualification of GMP-standard cryopreservative reagent for process improvement initiative

Biomedical Engineering Cellular Biomechanics Lab University Park, PA
Graduate Researcher *August 2013-Present*

- Developed and led experiments in vitro determining the effect of antibody-functionalized nanoparticles to target tumor cells and deliver chemotherapeutic drugs in dynamic flow environments
- Innovated new protocol for in vitro modified flow-migration device to test tumor cell adhesion and transendothelial migration
- Managed partnership with material science researchers to develop particles and conduct analysis on findings
- Selected to present poster at national 2015 Biomedical Engineering Society Meeting in Tampa, FL
- Funded by National Science Foundation REU grant, PSU College of Engineering Summer REU grant, and PSU Undergraduate Discover Grant

American Heart Association Summer Undergraduate Research Fellowship Hershey, PA
Intern *May 2013-August 2013*

- Selected in prestigious program of five undergraduate students funded by the American Heart Association to intern at the Penn State Milton S. Hershey Heart and Vascular Institute
- Conducted advanced analytics on the effects of oxidative stress on sympathetic vasoconstriction by measurement of muscle sympathetic nerve activity
- Employed signal-averaging technique on a beat-by-beat basis to determine mean arterial pressure increases after nerve activity bursts

LEADERSHIP EXPERIENCE

Bio-continuum Mechanics Course *August 2015-December 2015*
Grader

- Graded and proctored assessments for over 80 students for advanced undergraduate course

Schreyer Honors College Career Development Program *August 2014-December 2015*
Mentor

- Guided a group of five bioengineering students to advise on academic work and career trajectory

Women in Engineering Program Facilitated Study Group *January 2014-May 2014*
Group Facilitator

- Tutored a section of 12 undergraduate students in electricity and magnetism physics course on a weekly basis